Hydrol. Earth Syst. Sci., 21, 1669–1691, 2017
www.hydrol-earth-syst-sci.net/21/1669/2017/
doi:10.5194/hess-21-1669-2017

Hydrology and Earth System Sciences
Open Access
EGU

Identification of dominant hydrogeochemical processes for groundwaters in the Algerian Sahara supported by inverse modeling of chemical and isotopic data

Rabia Slimani[1], Abdelhamid Guendouz[2], Fabienne Trolard[3], Adnane Souffi Moulla[4], Belhadj Hamdi-Aïssa[1], and Guilhem Bourrié[3]

[1]Ouargla University, Fac. des Sciences de la Nature et de la Vie, Lab. Biochimie des Milieux Désertiques, 30000 Ouargla, Algeria
[2]Blida University, Science and Engineering Faculty, P.O. Box 270, Soumaâ, Blida, Algeria
[3]INRA – UMR1114 EMMAH, Avignon, France
[4]Algiers Nuclear Research Centre, P.O. Box 399, Alger-RP, 16000 Algiers, Algeria

Correspondence to: Rabia Slimani (slm_rabia@yahoo.fr)

Received: 8 September 2015 – Discussion started: 1 February 2016
Revised: 31 October 2016 – Accepted: 20 November 2016 – Published: 21 March 2017

Abstract. Unpublished chemical and isotopic data taken in November 1992 from the three major Saharan aquifers, namely the Continental Intercalaire (CI), the Complexe Terminal (CT) and the phreatic aquifer (Phr), were integrated with original samples in order to chemically and isotopically characterize the largest Saharan aquifer system and investigate the processes through which groundwaters acquire their mineralization. Instead of classical Debye–Hückel extended law, a specific interaction theory (SIT) model, recently incorporated in PHREEQC 3.0, was used. Inverse modeling of hydrochemical data constrained by isotopic data was used here to quantitatively assess the influence of geochemical processes: at depth, the dissolution of salts from the geological formations during upward leakage without evaporation explains the transitions from CI to CT and to a first end member, a cluster of Phr (cluster I); near the surface, the dissolution of salts from sabkhas by rainwater explains another cluster of Phr (cluster II). In every case, secondary precipitation of calcite occurs during dissolution. All Phr waters result from the mixing of these two clusters together with calcite precipitation and ion exchange processes. These processes are quantitatively assessed by the PHREEQC model. Globally, gypsum dissolution and calcite precipitation were found to act as a carbon sink.

1 Introduction

A scientific study published in 2008 (OECD, 2008) showed that 85 % of the world population lives in the driest half of the earth. More than 1 billion people residing in arid and semi-arid areas of the world have access to only few or nonrenewable water resources. The North-Western Sahara Aquifer System (NWSAS) is one of the largest confined reservoirs in the world and its huge water reserves are essentially composed of an old component. It is represented by two main deep aquifers, the Continental Intercalaire and the Complexe Terminal. This system covers a surface of more than 1 million km^2 (700 000 km^2 in Algeria, 80 000 km^2 in Tunisia and 250 000 km^2 in Libya). Due to the climatic conditions of Sahara, these formations are poorly renewed: about 1 billion m^3 yr^{-1} essentially infiltrated in the piedmont of the Saharan Atlas in Algeria, as well as in the Jebel Dahar and Jebel Nafusa in Tunisia and Libya, respectively. However, the very large extension of the system as well as the great thickness of the aquifer layers has favored the accumulation of huge water reserves. Ouargla basin is located in the middle of the NWSAS and thus benefits from groundwater resources (Fig. 1) which are contained in the following three main reservoirs (UNESCO, 1972; Eckstein and Eckstein, 2003; OSS, 2003, 2008):

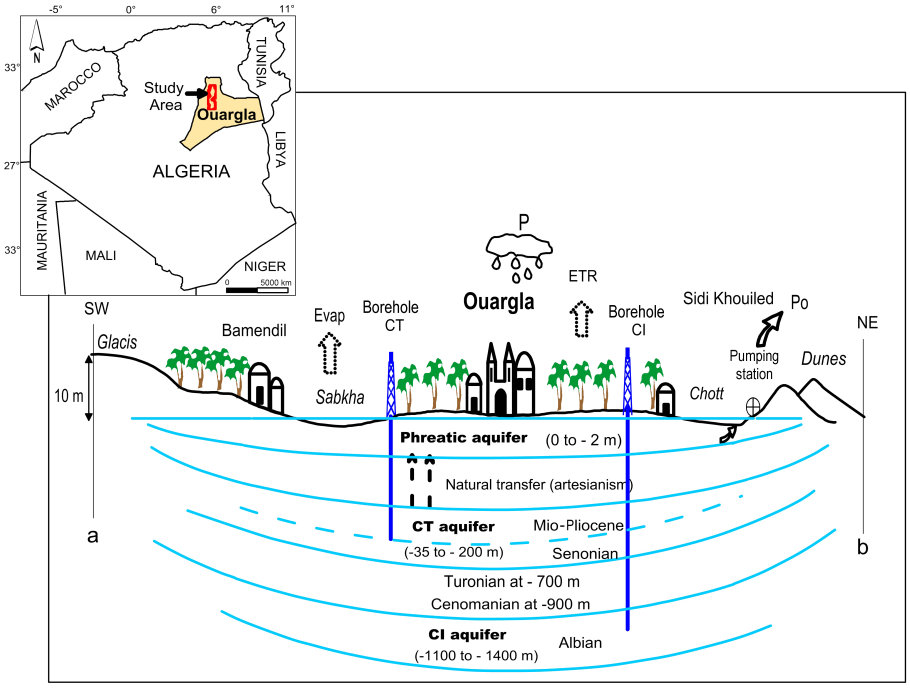

Figure 1. Location and schematic relations of aquifers in Ouargla. Blue lines represent limits between aquifers, and the names of aquifers are given in bold letters; as the limit between Senonian and Mio-Pliocene aquifers is not well defined, a dashed blue line is used. Names of villages and cities are given in roman (Bamendil, Ouargla, Sidi Khouiled), while geological/geomorphological features are in italic (glacis, sabkha, chott, dunes). Depths are relative to the ground surface. Letters "a" and "b" refer to the cross section (Fig. 2) and to the localization map (Fig. 3).

- At the top, the phreatic aquifer (Phr), in the Quaternary sandy gypsum permeable formations of Quaternary, is almost unexploited, due to its extreme salinity ($50\,g\,L^{-1}$).
- In the middle, the Complexe Terminal (CT) (Cornet and Gouscov, 1952; UNESCO, 1972) is the most exploited and includes several aquifers in different geological formations. Groundwater circulates in one or the two lithostratigraphic formations of the Eocene and Senonian carbonates or in the Mio-Pliocene sands.
- At the bottom, the Continental Intercalaire (CI), hosted in the lower Cretaceous continental formations (Barremian and Albian), mainly composed of sandstones, sands and clays. It is only partially exploited because of its significant depth.

The integrated management of these groundwaters is presently a serious issue for local water resources managers due to the large extension of the aquifers and the complexity of the relations between them. Several studies (Guendouz, 1985; Fontes et al., 1986; Guendouz and Moulla, 1996; Edmunds et al., 2003; Guendouz et al., 2003; Hamdi-Aïssa et al., 2004; Foster et al., 2006; OSS, 2008) started from chemical and isotopic information (^{2}H, ^{18}O, ^{234}U, ^{238}U, ^{36}Cl) to characterize the relationships between aquifers. In particular, such studies focused on the recharge of the deep CI aquifer system. These investigations especially dealt with water chemical facies, mapped iso-contents of various parameters and reported typical geochemical ratios ($[SO_4^{2-}]/[Cl^-]$, $[Mg^{2+}]/[Ca^{2+}]$) as well as other correlations. Minerals–solutions equilibria were checked by computing saturation indices with respect to calcite, gypsum, anhydrite and halite, but processes were only qualitatively assessed. The present study aims at applying for the first time ever in Algeria, inverse modeling to an extreme environment featuring a lack of data on a scarce natural resource (groundwater). New data were hence collected in order to characterize the hydrochemical and the isotopic composition of the major aquifers in the Saharan region of Ouargla. New possibilities offered by progress in geochemical modeling were used. The objective was also to identify the origin of the mineralization and the water-rock interactions that occur along the flow path. More specifically, inverse modeling of chemical reactions allows one to select the best conceptual model for the interpretation of the geochemical evolution of Ouargla aquifer system. The stepwise inversion strategy involves designing a list of scenarios (hypotheses) that take into consideration the most plausible combinations of geochemical processes that may occur within the studied medium. After resolving the scenarios in a stepwise manner, the one that provides the best conceptual geochemical model is then se-

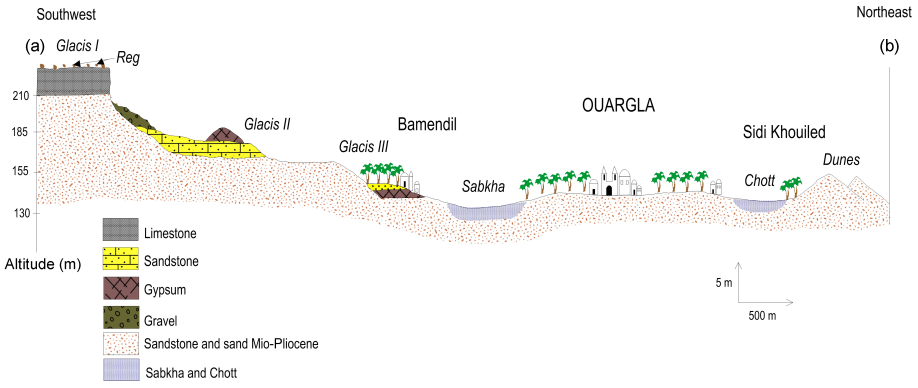

Figure 2. Geologic cross section in the region of Ouargla. The blue pattern used for chott and sabkha correspond to the limit of the saturated zone.

lected, which allowed Dai et al. (2006) to optimize simultaneously transmissivities and geochemical transformations in a confined aquifer. Inverse modeling with PHREEQC 3.0 was used here in a different way (only on geochemical data but for several aquifers) to account for the modifications of the composition of water along the flow path. At least two chemical analyses of groundwater at different points of the flow path, and a set of phases (minerals and/or gases) which potentially react while water circulates, are needed to operate the program (Charlton et al., 1996).

A number of assumptions are inherent to the application of inverse geochemical modeling: (i) the two groundwater analyses from the initial and the final boreholes should represent groundwater that flows along the same flow path; (ii) dispersion and diffusion do not significantly affect groundwater chemistry; (iii) a chemical steady state prevails in the groundwater system during the time considered; and (iv) the mineral phases used in the inverse calculation are or were present in the aquifer (Zhu and Anderson, 2002). The soundness or the validity of the results depends on a valid conceptualization of the groundwater system, on the validity of the basic hydrogeochemical concepts and principles, on the accuracy of model input data and on the level of understanding of the geochemical processes occurring in the area (Güler and Thyne, 2004; Sharif et al., 2008). These requirements are fulfilled in the region of Ouargla, which can be considered as a "window" to the largest Saharan aquifer, and thus one of the largest aquifers in the world in a semi-arid to hyper-arid region subject to both global changes: urban sprawl and climate change. The methodology developed here and the data collected can easily be integrated in the PRECOS framework proposed for the management of environmental resources (Trolard et al., 2016).

2 Methodology

2.1 Presentation of the study area

The study area is located in the northeastern desert of Algeria (lower Sahara) (Le Houérou, 2009) near the city of Ouargla (Fig. 1), 31°54′ to 32°1′ N and 5°15′ to 5°27′ E, with a mean elevation of 134 (m a.s.l.). It is located in the quaternary valley of Oued Mya basin. The present climate belongs to the arid Mediterranean type (Dubief, 1963; Le Houérou, 2009; ONM, 1975/2013), as it is characterized by a mean annual temperature of 22.5 °C, a yearly rainfall of 43.6 mm yr^{-1} and a very high evaporation rate of 2138 mm yr^{-1}.

Ouargla's region and the entire lower Sahara has experienced during its long geological history alternating marine and continental sedimentation phases. During Secondary era, vertical movements affected the Precambrian basement, causing, in particular, collapse of its central part, along an axis passing approximately through the Oued Righ Valley and the upper portion of the Oued Mya Valley. According to Furon (1960), a epicontinental sea spread to the Lower Eocene of northern Sahara. After the Oligocene, the sea gradually withdrew. It is estimated at present that this sea did not reach Ouargla and transgression stopped at the edge of the bowl (Furon, 1960; Lelièvre, 1969). The basin is carved into Mio-Pliocene (MP) deposits, which alternate with red sands, clays and sometimes marls; gypsum is not abundant and dated from the Pontian era (during the MP) (Cornet and Gouscov, 1952; Dubief, 1953; Ould Baba Sy and Besbes, 2006). The continental Pliocene consists of a local limestone crust with puddingstone or lacustrine limestone (Fig. 2), shaped by eolian erosion into flat areas (regs). The Quaternary formations are lithologically composed of alternating layers of permeable sand and relatively impermeable marl (Aumassip et al., 1972; Chellat et al., 2014).

The exploitation of Mio-Pliocene aquifer is ancient and at the origin of the creation of the oasis (Lelièvre, 1969; Moulias, 1927). The piezometric level was higher (145 m a.s.l.)

but overexploitation at the end of the 19th century led to a catastrophic decrease of the resource, with presently more than 900 boreholes (ANRH, 2011).

The exploitation of the Senonian aquifer dates back to 1953 at a depth between 140 and 200 m, with a small initial rate of approximately 9 L s^{-1}; two boreholes have been exploited since 1965 and 1969, with a total flow rate of approximately 42 L s^{-1}, for drinking water and irrigation.

The exploitation of the Albian aquifer dates back to 1956; presently, two boreholes are exploited:

- El Hedeb I, 1335 m deep, with a flow rate of 141 L s^{-1};
- El Hedeb II, 1400 m deep, with a flow rate of 68 L s^{-1}.

2.2 Sampling and analytical methods

The sampling programme consisted of collecting samples along transects corresponding to directions of flow for both the Phr and CT aquifers, while it was possible to collect only eight samples from the CI. A total of 107 samples were collected during a field campaign in 2013 along the main flow path of Oued Mya. Of these, 67 were from piezometers tapping the phreatic aquifer, 32 from CT wells and the last 8 from boreholes tapping the CI aquifer (Fig. 3). Analyses of Na^+, K^+, Ca^{2+}, Mg^{2+}, Cl^-, SO_4^{2-} and HCO_3^- were performed by ion chromatography at Algiers Nuclear Research Center (CRNA). Previous and yet unpublished data (Guendouz and Moulla, 1996) sampled in 1992 are used here too: 59 samples for the Phr aquifer, 15 samples for the CT aquifer and 3 samples for the CI aquifer for chemical analyses and data of ^{18}O and ^{3}H (Guendouz and Moulla, 1996).

2.3 Geochemical method

PHREEQC was used to check minerals–solutions equilibria using the specific interaction theory (SIT), i.e., the extension of Debye–Hückel law by Scatchard and Guggenheim incorporated recently in PHREEQC 3.0 (Parkhurst and Appelo, 2013). Inverse modeling was used to calculate the number of minerals and gases' moles that must, respectively, dissolve or precipitate/degas to account for the difference in composition between initial and final water end members (Plummer and Back, 1980; Kenoyer and Bowser, 1992; Deutsch, 1997; Plummer and Sprinckle, 2001; Güler and Thyne, 2004; Parkhurst and Appelo, 2013). This mass balance technique has been used to quantify reactions controlling water chemistry along flow paths (Thomas et al., 1989). It is also used to quantify the mixing proportions of end-member components in a flow system (Kuells et al., 2000; Belkhiri et al., 2010, 2012).

Inverse modeling involves designing a list of scenarios (modeling setups) that take into account the most plausible combinations of geochemical processes that are likely to occur in our system. For example, the way to identify whether calcite dissolution/precipitation is relevant or not consists of solving the inverse problem under two alternate scenarios: (1) considering a geochemical system in which calcite is present and (2) considering a geochemical system without calcite. After simulating the two scenarios, it is usually possible to select the setup that gives the best results as the solution to the inverse modeling according to the fit between the modeled and observed values. Then one can conclude whether calcite dissolution/precipitation is relevant or not. This stepwise strategy allows us to identify the relevance of a given chemical process by inversely solving the problem through alternate scenarios in which the process is either participating or not (Dai et al., 2006).

In the geochemical modeling inverse, soundness of results is dependent upon valid conceptualization of the system, validity of basic concepts and principles, accuracy of input data and level of understanding of the geochemical processes. We use the information from the lithology, general hydrochemical evolution patterns, saturation indices and mineral stability diagrams to constrain the inverse models.

3 Results and discussion

Tables 1 to 4 illustrate the results of the chemical and the isotopic analyses. Samples are ordered according to an increasing electric conductivity (EC), and this is assumed to provide an order for increasing salt content. In both the phreatic and CT aquifers, temperature is close to 25 °C, while for the CI aquifer, temperature is close to 50 °C. The values presented in Tables 1 to 5 are raw analytical data that were corrected for defects of charge balance before computing activities with PHREEQC. As analytical errors could not be ascribed to a specific analyte, the correction was made proportionally. The corrections do not affect the anion-to-anion mole ratios, such as for $[HCO_3^-]/([Cl^-]+2[SO_4^{2-}])$ or $[SO_4^{2-}]/[Cl^-]$, whereas they affect the cation-to-anion ratio, such as for $[Na^+]/[Cl^-]$.

3.1 Characterization of chemical facies of the groundwater

Piper diagrams drawn for the studied groundwaters (Fig. 4) broadly show a scatter plot dominated by a sodium chloride facies. However, when going into small details, the widespread chemical facies of the Phr aquifer are closer to the NaCl cluster than those of the CI and CT aquifers. Respectively, $CaSO_4$, Na_2SO_4, $MgSO_4$ and NaCl are the most dominant chemical species (minerals) that are present in the phreatic waters. This sequential order of solutes is comparable to that of other groundwater occurring in north Africa and especially in the neighboring area of the chotts (depressions where salts concentrate by evaporation) Merouane and Melrhir (Vallès et al., 1997; Hamdi-Aïssa et al., 2004).

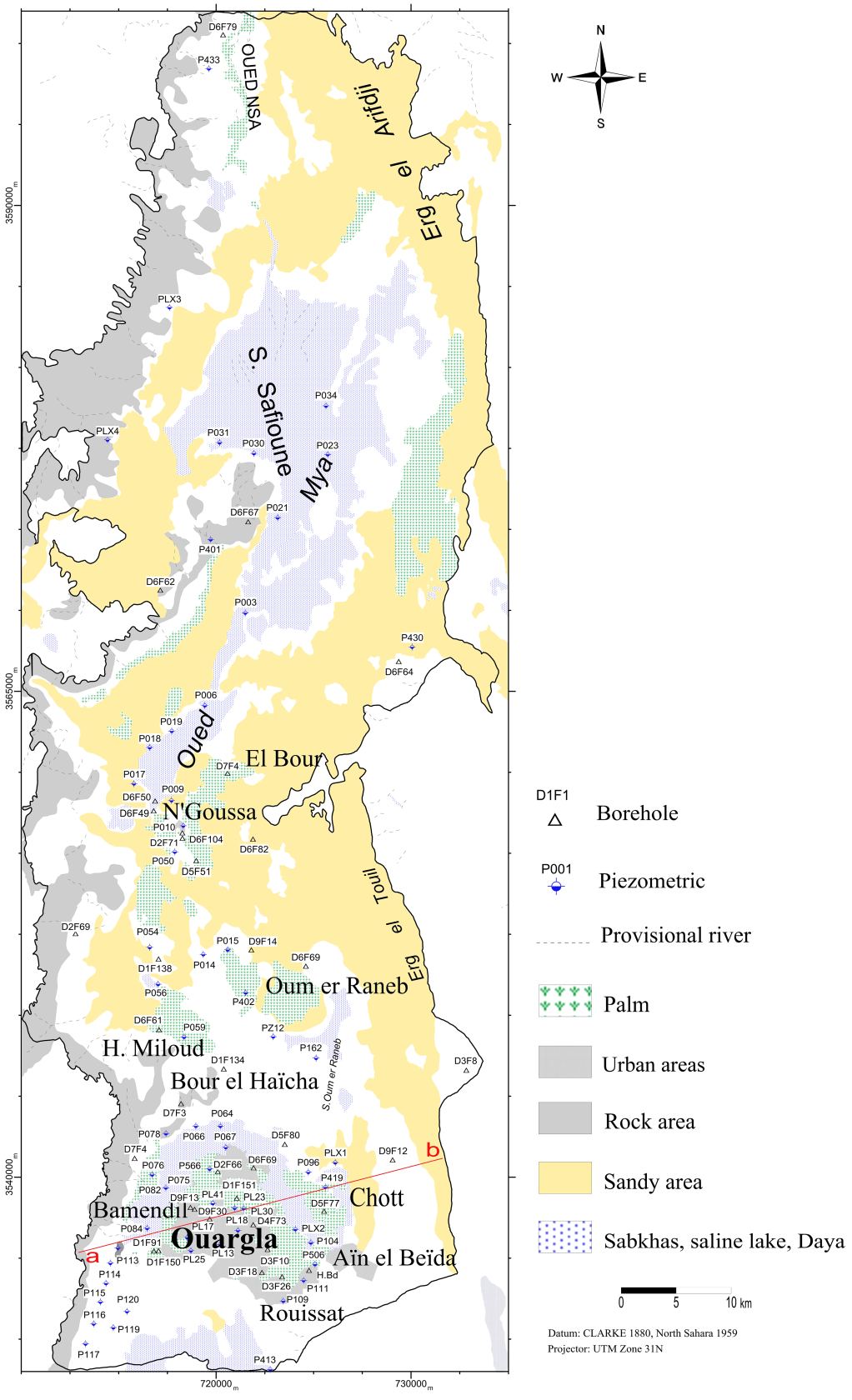

Figure 3. Location map of sampling points.

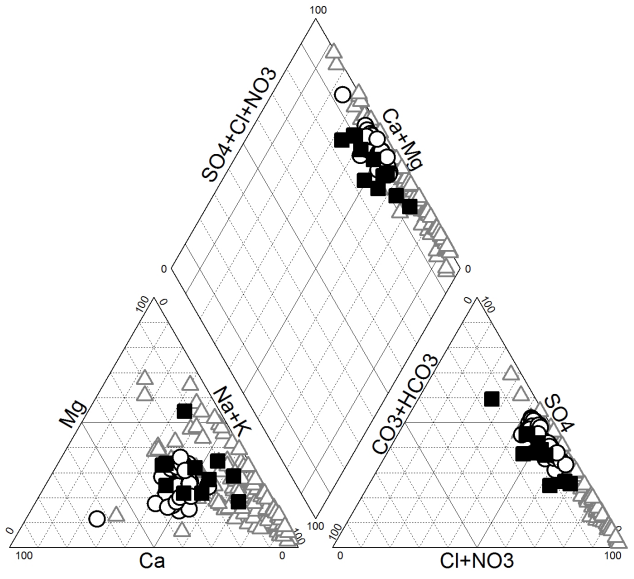

Figure 4. Piper diagram for the Continental Intercalaire (filled squares), Complexe Terminal (open circles) and phreatic (open triangles) aquifers.

3.2 Spatial distribution of the mineralization

The salinity of the phreatic aquifer varies considerably depending on the location (namely, the distance from wells or drains) and time (due to the influence of irrigation) (Fig. 5a).

Its salinity is low around irrigated and fairly well-drained areas, such as the palm groves of Hassi Miloud, just north of Ouargla (Fig. 3), that benefit from freshwater and are drained to the sabkha Oum El Raneb. However, the three lowest salinity values are observed in the wells of the Ouargla palm grove itself, where the Phr aquifer water table is deeper than 2 m.

Conversely, the highest salinity waters are found in wells drilled in the chotts and sabkhas (a sabkha is the central part of a chott where salinity is the largest) (Safioune and Oum er Raneb) where the aquifer is often shallower than 50 cm.

The salinity of the CT (Mio-Pliocene) aquifer (Fig. 5b) is much lower than that of the Phr aquifer and ranges from 1 to $2\,g\,L^{-1}$; however, its hardness is larger and it contains more sulfate, chloride and sodium than the waters of the Senonian formations and those of the CI aquifer. The salinity of the Senonian aquifer ranges from 1.1 to $1.7\,g\,L^{-1}$, while the average salinity of the CI aquifer is $0.7\,g\,L^{-1}$ (Fig. 5c).

A likely contamination of the Mio-Pliocene aquifer by phreatic groundwaters through casing leakage in an area where water is heavily loaded with salt, and therefore particularly aggressive, cannot be excluded.

3.3 Saturation indices

The calculated saturation indices (SIs) reveal that waters from CI at 50 °C are close to equilibrium with respect to calcite, except for three samples that are slightly oversaturated. They are, however, all undersaturated with respect to gypsum (Fig. 6).

Moreover, they are oversaturated with respect to dolomite and undersaturated with respect to anhydrite and halite (Fig. 7).

Waters from the CT and phreatic aquifers show the same pattern, but some of them are more largely oversaturated with respect to calcite, at 25 °C.

However, several phreatic waters (P031, P566, PLX4, PL18, P002, P023, P116, P066, P162 and P036) that are located in the sabkhas of Safioune, Oum er Raneb, Bamendil and Aïn el Beïda's chott are saturated with gypsum and anhydrite. This is in accordance with highly evaporative environments found elsewhere (UNESCO, 1972; Hamdi-Aïssa et al., 2004; Slimani, 2006).

No significant trend of SI from south to north upstream and downstream of Oued Mya (Fig. 7) is observed. This suggests that the acquisition of mineralization is due to geochemical processes that have already reached equilibrium or steady state in the upstream areas of Ouargla.

3.4 Change of facies from the carbonated cluster to the evaporites' cluster

The facies shifts progressively from the carbonated cluster (CI and CT aquifers) to the evaporites' cluster (Phr aquifer) with an increase in sulfates and chlorides at the expense of carbonates (SI of gypsum, anhydrite and halite). This is illustrated by a decrease of the $[HCO_3^-]/([Cl^-]+2[SO_4^{2-}])$ ratio (Fig. 8) from 0.2 to 0 and of the $[SO_4^{2-}]/[Cl^-]$ ratio from 0.8 to values smaller than 0.3 (Fig. 9) while salinity increases. Carbonate concentrations tend towards very small values, while it is not the case for sulfates. This is due to both gypsum dissolution and calcite precipitation. Chlorides in groundwater may come from three different sources: (i) ancient sea water entrapped in sediments, (ii) dissolution of halite and related minerals that are present in evaporite deposits and (iii) dissolution of dry fallout from the atmosphere, particularly in these arid regions (Matiatos et al., 2014; Hadj-Ammar et al., 2014).

The $[Na^+]/[Cl^-]$ ratio ranges from 0.85 to 1.26 for the CI aquifer, from 0.40 to 1.02 for the CT aquifer and from 0.13 to 2.15 for the Phr aquifer. The measured points from the three considered aquifers are linearly scattered with good approximation around the unity slope straight line that stands for halite dissolution (Fig. 10). The latter appears as the most dominant reaction occurring in the medium. However, at very high salinity, Na^+ seems to swerve from the straight line towards smaller values.

A further scrutiny of Fig. 10 shows that CI waters are very close to the 1 : 1 line. CT waters are enriched in both Na^+ and Cl^- but slightly lower than the 1 : 1 line while phreatic waters are largely enriched and much more scattered. CT waters are closer to the seawater mole ratio (0.858), but some lower values imply a contribution from a source of

Table 1. Field and analytical data for the Continental Intercalaire aquifer.

Locality	Lat.	Long.	Elev.	Date	EC	T	pH	Alk.	Cl^-	SO_4^{2-}	Na^+	K^+	Mg^{2+}	Ca^{2+}	Br^-
	(m)				(mS cm^{-1})	(°C)		(mmol L^{-1})							
Hedeb I	3 534 750	723 986	134	9 Nov 2012	2.0	46.5	7.6	3.5	5.8	6.8	10.7	0.6	2.5	3.3	0.034
Hedeb I	3 534 750	723 986	134	1992	1.9	49.3	7.3	0.4	5.8	1.1	5.7	0.2	0.8	0.5	
Hedeb II	3 534 310	724 290	146	1992	2.0	47.4	7.6	0.6	6.2	1.2	5.1	0.2	1.3	0.8	
Aouinet Moussa	3 548 896	721 076	132	1992	2.2	48.9	7.5	1.3	6.5	1.9	5.6	0.2	1.1	1.2	
Aouinet Moussa	3 548 896	721 076	132	22 Feb 2013	2.2	48.9	7.5	3.2	9.8	3.9	6.3	0.7	5.7	1.3	
Hedeb I	3 534 750	723 986	134	11 Dec 2010	2.2	49.3	7.3	1.9	12.4	4.6	10.7	0.7	3.8	2.3	
Hedeb II	3 534 310	724 290	146	11 Dec 2010	2.2	47.4	7.6	2.1	13.1	5.5	13.9	0.5	4.5	1.4	
Hassi Khfif	3 591 659	721 636	110	24 Feb 2013	2.4	50.5	6.8	2.9	14.3	5.2	10.8	0.8	3.4	4.6	0.033
Hedeb I	3 534 750	723 986	134	27 Feb 2013	2.0	46.5	7.6	3.5	15.1	7.7	11.8	0.5	5.6	5.2	
Hassi Khfif	3 591 659	721 636	110	9 Nov 2012	2.2	50.1	7.6	3.3	15.3	7.8	12.2	0.6	5.8	4.9	
El Bour	3 560 264	720 366	160	22 Feb 2013	2.9	54.5	7.3	2.6	18.6	6.2	20.6	0.7	4.8	1.4	

chloride other than halite or from entrapped seawater. Conversely, a $[Na^+]/[Cl^-]$ ratio larger than 1 is observed for phreatic waters, which implies the contribution of another source of sodium, most likely sodium sulfate, that is present as mirabilite or thenardite in the chotts and the sabkha areas.

The $[Br^-]/[Cl^-]$ ratio ranges from 2×10^{-3} to 3×10^{-3}. The value of this molar ratio for halite is around 2.5×10^{-3}, which matches the aforementioned range and confirms that halite dissolution is the most dominant reaction taking place in the studied medium.

In the CI, CT and Phr aquifers, calcium originates both from carbonate and sulfate (Figs. 11 and 12). Three samples from the CI aquifer are close to the $[Ca^{2+}]/[HCO_3^-]$ 1 : 2 line, while calcium sulfate dissolution explains the excess of calcium. However, nine samples from the Phr aquifer are depleted in calcium, and plotted under the $[Ca^{2+}]/[HCO_3^-]$ 1 : 2 line. This cannot be explained by precipitation of calcite, as some are undersaturated with respect to that mineral, while others are oversaturated.

In this case, a cation exchange process seems to occur and lead to a preferential adsorption of divalent cations, with a release of Na^+. This is confirmed by the inverse modeling that is developed below and which implies Mg^{2+} fixation and Na^+ and K^+ releases.

Larger sulfate values observed in the phreatic aquifer (Fig. 12) with $[Ca^{2+}]/[SO_4^{2-}] < 1$ can be attributed to a Na-Mg sulfate dissolution from a mineral bearing such elements. This is, for instance, the case of bloedite.

3.5 Isotope geochemistry

The CT and CI aquifers exhibit depleted and homogeneous ^{18}O contents, ranging from −8.32 to −7.85 ‰. This was already previously reported by many authors (Edmunds et al., 2003; Guendouz et al., 2003; Moulla et al., 2012). On the other hand, ^{18}O values for the phreatic aquifer are widely dispersed and vary between −8.84 and 3.42 ‰ (Table 4). Waters located north of the virtual line connecting, approximately, Hassi Miloud to Sebkhet Safioune, are found more enriched in heavy isotopes and are thus more evaporated. In that area, the water table is close to the surface and mixing of both CI and CT groundwaters with phreatic ones through irrigation is nonexistent. Conversely, waters located south of Hassi Miloud up to Ouargla city show depleted values. This is the clear fingerprint of a contribution to the Phr waters from the underlying CI and CT aquifers (Gonfiantini et al., 1975; Guendouz, 1985; Fontes et al., 1986; Guendouz and Moulla, 1996).

Phreatic waters result from a mixing of two end members. Evidence for this is given by considering the $[Cl^-]$ and ^{18}O relationship (Fig. 13). The two clusters are (i) a first cluster of ^{18}O-depleted groundwater (Fig. 14), and (ii) another cluster of ^{18}O-enriched groundwater with positive values and a high salinity. The latter is composed of phreatic waters occurring in the northern part of the study region.

Table 2. Field and analytical data for the Complexe Terminal aquifer.

Locality	Site	Aquifer	Lat.	Long.	Elev.	Date	EC	T	pH	Alk.	Cl^-	SO_4^{2-}	Na^+	K^+	Mg^{2+}	Ca^{2+}	Br^-
			(m)				(mS cm^{-1})	(°C)		(mmol L^{-1})							
Bamendil	D7F4	M	3 560 759	720 586	296	20 Jan 2013	2.0	20.1	7.9	1.6	10.1	5.8	9.9	0.7	3.9	2.5	
Bamendil	D7F4	M	3 560 759	720 586	296	1992	2.0	21.1	8.2	0.9	10.6	3.5	10.6	0.1	2.3	1.8	
Ifri	D1F151	S	3 538 891	721 060	204	1992	2.7	23.5	7.0	1.3	10.7	2.7	8.0	0.7	2.3	2.1	
Said Otba	D2F66	S	3 540 257	720 085	216	1992	2.3	24.0	8.0	1.4	11.0	4.7	11.5	0.2	2.1	3.3	
Oglat Larbaâ	D6F64	M	3 566 501	729 369	177	1992	2.3	18.0	7.9	1.4	11.4	6.8	11.6	2.3	2.0	4.6	
El Bour	D4F94	M	3 536 245	722 641	100	27 Jan 2013	3.1	26.2	7.4	1.6	12.8	6.8	5.2	1.9	1.6	9.1	
Said Otba I	D2F71	S	3 557 412	718 272	211	1992	2.3	24.2	8.2	1.5	13.5	5.7	15.0	0.3	3.3	2.6	
Debiche	D6F61	M	3 547 557	717 067	173	26 Jan 2013	2.2	23.9	7.7	1.8	14.2	8.4	12.6	0.7	5.4	4.4	
Rouissat III	D3F10	S	3 535 068	722 352	248	1992	3.1	26.1	7.3	2.4	14.3	6.9	13.1	0.4	3.4	5.4	
Said Otba I	D2F71	S	3 557 412	718 272	212	26 Jan 2013	5.6	25.1	7.3	2.4	14.3	6.9	13.1	0.4	3.4	5.4	0.034
Rouissat III	D3F10	S	3 535 068	722 352	248	20 Jan 2013	2.3	18.9	8.0	1.6	15.2	8.6	12.6	1.6	5.8	4.3	
Ifri	D1F151	S	3 538 891	72 1060	204	27 Jan 2013	2.4	22.9	7.8	1.7	15.4	8.3	13.7	0.2	5.2	4.8	
Said Otba	D2F66	S	3 540 257	720 085	216	31 Jan 2013	2.4	24.9	7.9	2.2	16.1	8.6	16.5	0.7	4.9	4.3	
Oglat Larbaâ	D6F64	M	3 566 501	729 369	177	31 Jan 2013	2.4	23.7	7.6	2.3	16.3	8.6	13.6	0.7	5.9	5.0	
SAR Mekhadma	D1F91	S	3 536 757	717 822	221	3 Feb 2013	2.5	25.8	7.7	3.4	16.5	8.5	16.1	0.7	5.3	4.9	
Sidi Kouiled	D9F12	S	3 540 855	729 055	329	24 Jan 2013	2.6	21.3	8.1	4.6	16.8	8.8	16.1	0.8	6.2	5.0	
Aïn N'Sara	D6F50	S	3 559 323	716 868	255	25 Jan 2013	3.4	25.7	7.4	2.0	16.9	9.7	15.9	0.3	3.4	7.9	0.033
A. Louise	D4F73	S	3 537 523	721 904	310	26 Jan 2013	2.6	24.0	7.5	2.0	17.4	9.1	13.9	2.0	5.8	5.1	
Ghâzalet A. H	D6F79	M	3 598 750	720 356	119	2 Feb 2013	2.8	22.5	7.5	3.5	17.4	9.3	16.6	0.6	6.2	4.9	
Aïn Moussa II	D9F30	S	3 537 814	719 665	220	2 Feb 2013	7.5	23.9	7.5	2.4	17.5	8.2	17.3	0.4	3.1	6.5	0.033
Aïn N'Sara	D6F50	S	3 559 323	716 868	255	2 Feb 2013	2.6	23.8	7.6	2.1	17.7	9.2	15.5	1.1	6.1	4.7	
H. Miloud	D1F135	M	3 547 557	717 067	173	3 Feb 2013	2.8	21.6	7.5	3.3	17.9	9.2	16.5	1.0	6.2	4.9	
El Bour	D6F97	S	3 540 936	715 816	169	25 Jan 2013	2.6	19.9	8.0	2.1	17.9	9.3	15.8	1.6	5.8	4.7	
H. Miloud	D1F135	M	3 547 557	717 067	173	1992	2.1	22.7	8.1	2.8	18.1	5.7	16.6	0.5	3.6	4.3	
N'Goussa El Hou	D6F51	S	3 556 256	718 979	198	31 Jan 2013	2.9	22.9	7.5	2.0	18.4	9.6	17.1	0.5	6.2	5.0	
El Koum	D6F67	S	3 573 694	721 639	143	21 Jan 2013	3.1	22.9	8.1	3.5	18.4	9.7	17.9	0.3	6.5	5.1	
El Koum	D6F67	S	3 573 694	721 639	143	1992	2.5	25.0	7.6	1.5	18.8	7.2	10.2	3.4	5.0	5.8	
Itas	D1F150	M	3 536 186	717 046	93	21 Jan 2013	3.7	23.9	7.5	1.5	18.8	7.1	10.1	3.4	5.0	5.8	
Aïn Moussa V	D9F13	M	3 538 409	718 680	210	8 Feb 2013	2.4	25.3	7.2	2.3	19.4	9.4	18.8	0.4	3.3	7.6	0.034
El Bour	D4F94	M	3 536 245	722 641	100	1992	2.3	21.2	7.9	1.6	20.1	7.2	12.1	2.6	5.8	5.2	
Rouissat I	D3F18	M	3 535 564	722 498	80	26 Jan 2013	3.1	23.0	8.1	3.2	21.2	11.1	19.6	0.9	7.1	6.0	
Rouissat I	D3F18	M	3 535 564	722 498	80	1992	2.0	20.0	7.8	1.7	21.7	8.5	17.7	1.2	5.1	6.0	
Station de Pompage chott	D5F80	S	3 541 656	723 521	224	4 Feb 2013	3.3	24.5	8.2	3.9	22.1	11.9	19.9	2.1	7.6	6.3	
Chott Palmeraie	D5F77	S	3 538 219	725 541	243	5 Feb 2013	3.4	24.6	7.5	3.3	22.3	12.1	20.9	1.2	8.3	5.8	
Bour el Aïcha	D1F134	M	3 545 533	720 391	86	5 Feb 2013	3.4	22.2	7.3	4.1	23.2	12.2	21.2	1.5	8.6	6.0	
Abazat	D2F69	M	3 552 504	712 786	137	3 Feb 2013	3.5	24.6	7.6	2.2	24.7	12.7	21.1	1.7	8.5	6.5	
Garet Chemia	D1F113	S	3 536 174	716 808	213	28 Jan 2013	4.1	28.0	7.3	2.2	25.9	9.5	25.4	0.6	3.6	7.2	0.037
Frane	D6F62	M	3 570 175	717 133	167	27 Jan 2013	3.8	24.2	7.9	2.3	25.9	13.5	22.6	0.6	8.9	7.2	

Table 2. Continued.

Locality	Site	Aquifer	Lat.	Long.	Elev.	Date	EC	T	pH	Alk.	Cl^-	SO_4^{2-}	Na^+	K^+	Mg^{2+}	Ca^{2+}	Br^-
			(m)				($mS\,cm^{-1}$)	(°C)		($mmol\,L^{-1}$)							
Oum er Raneb	D6 F69	M	3 540 451	721 919	216	25 Jan 2013	4.2	24.1	7.0	2.6	27.9	8.7	22.9	0.6	4.4	8.0	0.035
N'Goussa El Hou	D6F51	S	3 556 256	718 979	198	1992	3.1	23.2	8.0	2.6	28.4	8.6	23.1	0.6	4.5	8.0	
H. Miloud Benyaza	D1F138	M	3 551 192	717 042	89	28 Jan 2013	3.8	25.2	7.6	2.4	28.4	14.2	23.9	1.7	10.0	7.1	
Aïn Larbaâ	D6F49	M	3 558 822	716 799	156	28 Jan 2013	3.9	23.7	7.3	2.2	28.9	9.0	23.9	0.5	5.0	7.7	0.037
H. Miloud Benyaza	D1F138	M	3 551 192	717 042	89	1992	2.9	22.8	7.5	2.2	28.9	9.1	23.9	0.5	5.0	7.7	
Rouissat	D3F8	M	3 545 470	732 837	332	3 Feb 2013	4.4	25.4	7.5	1.7	29.8	8.3	22.8	1.2	6.2	6.1	
Rouissat	D3F8	M	3 545 470	732 837	332	1992	6.2	25.3	7.2	1.7	29.8	8.3	22.9	1.2	6.2	6.1	
Aïn El Arch	D3F26	M	3 534 843	723 381	93	1992	5.1	25.1	7.4	1.6	34.7	8.9	24.0	0.9	8.4	6.5	
Station de Pompage chott	D5F80	S	3 541 656	723 521	224	1992	3.7	25.4	7.7	2.3	42.2	13.5	36.8	1.1	7.4	9.7	

M = Mio-Pliocene aquifer; S = Senonian aquifer.

Cluster I represents the waters from CI and CT whose isotopic composition is depleted in ^{18}O (average value around $-8.2\,‰$) (Fig. 13). They correspond to an old water recharge (paleo-recharge), whose age, estimated by means of ^{14}C, exceeds 15 000 yr BP (Guendouz, 1985; Guendouz and Michelot, 2006). Thus, it is not a water body that is recharged by recent precipitation. It consists of CI and CT groundwaters and partly of phreatic waters and can be ascribed to an upward leakage favored by the extension of faults near Amguid El Biod dorsal.

Cluster II, observed in Sebkhet Safioune, can be ascribed to the direct dissolution of surficial evaporitic deposits conveyed by evaporated rainwater.

Evaporation alone cannot explain the distribution of data that is observed (Fig. 13). Evidence for this is given in a semi-logarithmic plot (Fig. 14), as classically obtained according to the simple approximation of the Rayleigh equation (cf. Appendix):

$$\begin{aligned}\delta^{18}\mathrm{O} &\approx 1000 \times (1-\alpha)\log\left[\mathrm{Cl}^-\right] + k,\\ &\approx -\epsilon \log\left[\mathrm{Cl}^-\right] + k,\end{aligned} \tag{1}$$

where α is the fractionation factor during evaporation, $\epsilon \equiv -1000 \times (1-\alpha)$ is the enrichment factor and k is a constant (Ma et al., 2010; Chkir et al., 2009). CI and CT waters are better separated in the semi-logarithmic plot because they are differentiated by their chloride content. According to Eq. (1), simple evaporation gives a straight line (solid line in Fig. 14). The value of ϵ used is the value at 25 °C, which is equal to −73.5.

P115 is the only sample that appears on the straight evaporation line (Fig. 14). It should be considered as an outlier since the rest of the samples are all well aligned on the logarithmic fit derived from the mixing line of Fig. 13.

The phreatic waters that are close to cluster I (Fig. 13) correspond to groundwaters occurring in the edges of the basin (Hassi Miloud, piezometer P433) (Fig. 14). They are low mineralized and acquire their salinity via two processes, namely dissolution of evaporites along their underground transit up to Sebkhet Safioune and dilution through upward leakage by the less-mineralized waters of the CI and CT aquifers (for example, Hedeb I for CI and D7F4 for CT) (Fig. 14) (Guendouz, 1985; Guendouz and Moulla, 1996).

The rates of the mixing that are due to upward leakage from CI to CT towards the phreatic aquifer can be calculated by means of a mass balance equation. It only requires knowing the δ values of each fraction that is involved in the mixing process.

The δ value of the mixture is given by

$$\delta_{\mathrm{mix}} = f \times \delta_1 + (1-f) \times \delta_2, \tag{2}$$

where f is the fraction of the CI aquifer, $1-f$ the fraction of the CT and δ_1, δ_2 are the respective isotope contents.

Table 3. Field and analytical data for the phreatic aquifer.

Locality	Site	Lat.	Long.	Elev.	Date	EC	T	pH	Alk.	Cl^-	SO_4^{2-}	Na^+	K^+	Mg^{2+}	Ca^{2+}	Br^-
			(m)			($mS\,cm^{-1}$)	(°C)		($mmol\,L^{-1}$)							
Bou Khezana	P433	3 597 046	719 626	118	20 Jan 2013	2.1	22.7	9.2	1.6	12.0	7.3	13.0	1.0	4.3	2.8	
Bou Khezana	P433	3 597 046	719 626	118	1992	2.0	22.1	8.9	1.5	12.0	6.9	11.6	0.9	4.4	2.9	
Hassi Miloud	P059	3 547 216	718 358	124	27/01/2013	2.1	23.9	8.2	1.9	13.0	7.3	12.6	1.3	4.4	3.4	0.024
Aïn Kheir	PL06				1992	4.0	23.8	7.5	1.9	14.2	17.9	15.9	0.6	10.6	7.5	
Hassi Naga	PLX3	3 584 761	717 604	125	20 Jan 2013	2.9	23.0	8.1	2.0	17.7	9.4	16.6	0.9	5.8	5.0	0.031
	LTP 30				1992	4.1	23.7	7.1	5.3	18.2	10.0	24.3	0.4	1.4	8.1	
Maison de culture	PL31	3 537 988	720 114	124	1992	2.5	23.8	8.1	1.5	18.9	7.8	26.1	0.6	2.1	3.0	
El Bour	P006	3 564 272	719 421	161	1992	3.0	23.4	7.9	1.3	19.0	7.7	12.4	2.7	5.3	5.3	
Hassi Miloud	P059	3 547 216	718 358	124	1992	2.8	23.5	7.8	2.3	20.8	9.4	34.2	4.3	1.4	0.9	
Oglat Larbaâ	P430	3 567 287	730 058	139	24 Jan 2013	4.5	27.5	8.3	3.3	22.1	12.4	21.8	2.6	8.6	5.5	
Maison de culture	PL31	3 537 988	720 114	124	28 Jan 2013	3.7	22.2	8.2	4.2	22.6	8.6	28.4	2.2	4.0	3.2	
Frane El Koum	P401	3 572 820	719 721	112	20 Jan 2013	3.4	27.5	7.5	2.2	23.3	13.4	21.8	1.9	8.3	6.3	0.032
Gherbouz	PL15	3 537 962	718 744	134	1992	2.5	23.5	7.7	3.0	23.5	14.0	50.6	2.8	1.0	0.3	
Bour El Haïcha	P408	3 544 999	719 930	110	1992	2.4	23.5	7.8	2.4	24.2	13.2	41.9	6.1	2.3	0.8	
Station d'épuration	PL30	3 538 398	721 404	130	1992	5.5	23.8	7.4	3.0	24.3	21.2	24.3	0.9	20.2	2.2	
Frane Ank Djemel	P422	3 575 339	718 875	109	20 Jan 2013	4.1	24.2	8.4	4.4	25.3	9.5	23.7	1.8	4.2	7.9	0.025
Route Aïn Beïda	PLX2	3 537 323	724 063	127	1992	4.7	23.6	7.2	2.0	25.7	10.4	14.8	0.2	9.3	7.4	
H. Chegga	PLX4	3 577 944	714 428	111	20 Jan 2013	4.1	25.2	7.6	3.0	26.2	9.8	24.0	2.3	5.0	7.5	0.033
Hassi Miloud	P058	3 547 329	716 520	129	27 Jan 2013	3.7	24.6	8.1	3.0	27.7	10.6	19.0	2.3	9.1	6.6	0.033
Route Aïn Moussa	P057	3 548 943	717 353	133	1992	5.3	23.4	7.7	1.3	28.2	11.5	17.6	2.0	11.5	5.8	
Route El Goléa	P115	3 533 586	714 060	141	1992	2.6	23.7	7.6	2.8	28.8	14.5	58.7	0.1	0.8	0.7	
Mekhadma	PL05	3 537 109	718 419	137	1992		23.9	7.8	1.7	30.9	16.7	24.9	1.0	15.7	4.5	
Polyclinique Bel Abbès	PL18	3 537 270	721 119	119	31/01/2013	4.7	22.2	7.9	1.8	31.2	15.4	21.3	3.9	11.2	8.4	
H. Chegga	PLX4	3 577 944	714 428	111	1992	4.5	23.7	7.6	1.5	31.5	10.1	20.1	5.9	7.5	6.5	
Route El Goléa	P116	3 532 463	713 715	117	1992	5.6	23.7	7.6	1.4	31.9	12.8	22.2	0.8	10.6	8.0	
Gherbouz	PL15	3 537 962	718 744	134	21 Jan 2013	4.7	23.3	8.2	1.8	32.4	14.6	27.8	0.8	6.8	10.8	
Route El Goléa	P117	3 531 435	713 298	111	1992	4.7	23.7	7.7	1.5	32.8	12.8	30.2	1.0	9.2	5.7	
Route Aïn Moussa	P057	3 548 943	717 353	133	26 Jan 2013	5.7	26.2	7.6	2.5	33.5	11.9	27.7	5.9	6.0	7.6	
Ecole Paramédicale	PL32	3 538 478	720 170	131	21 Jan 2013	5.7	22.9	8.2	2.0	33.6	12.1	29.2	3.3	6.4	8.2	
Direction des Services Agricoles	PL10	3 537 055	719 746	114	1992	6.1	23.7	7.7	1.3	35.0	13.5	8.6	1.9	19.4	7.2	
Route El Goléa	P117	3 531 435	713 298	111	3 Feb 2013	5.5	25.0	7.7	3.3	35.4	13.8	37.1	3.0	8.4	5.7	
Route El Goléa	P116	3 532 463	713 715	117	3 Feb 2013	5.8	22.5	8.1	1.7	36.3	11.6	28.5	3.2	6.8	8.4	
Station d'épuration	PL30	3 538 398	721 404	130	31 Jan 2013	5.3	25.1	7.8	4.1	38.4	14.6	28.5	4.5	11.6	8.1	
Hassi Debiche	P416	3 581 097	730 922	106	24 Jan 2013	5.5	23.7	8.8	0.3	38.6	18.0	22.3	0.9	4.8	21.3	
Direction des Services Agricoles	PL10	3 537 055	719 746	114	28 Jan 2013	5.5	24.6	8.4	2.4	38.8	16.9	36.9	1.9	9.1	9.2	
Hôpital	LTPSN2	3 538 292	720 442	132	27 Jan 2013	6.1	25.4	7.8	1.6	39.7	11.7	36.0	8.4	5.1	6.0	
Parc SONACOM	PL28	3 536 077	719 558	134	21 Jan 2013	6.1	24.5	8.1	1.8	39.8	11.8	30.6	5.2	7.1	8.5	
Bour El Haïcha	P408	3 544 999	719 930	110	27 Jan 2013	6.2	23.1	8.1	1.8	42.0	19.1	27.5	13.2	13.4	8.1	
Route Aïn Moussa	P056	3 549 933	717 022	128	1992	7.6	23.6	7.9	0.6	42.1	10.7	18.9	1.9	12.6	9.3	
Route Aïn Moussa	P056	3 549 933	717 022	128	26 Jan 2013	6.0	24.6	7.6	2.2	42.5	17.9	32.1	8.0	12.5	8.1	

Table 3. Continued.

Locality	Site	Lat.	Long.	Elev.	Date	EC	T	pH	Alk.	Cl^-	SO_4^{2-}	Na^+	K^+	Mg^{2+}	Ca^{2+}	Br^-
			(m)			($mS\,cm^{-1}$)	(°C)						($mmol\,L^{-1}$)			
Ecole Okba B. Nafaa	PL41	3 538 660	719 831	127	31 Jan 2013	6.3	24.1	7.7	2.1	44.9	13.2	36.2	11.8	6.3	6.7	
Parc Hydraulique	P419	3 539 494	725 605	132	31 Jan 2013	7.0	26.4	7.8	2.1	45.1	14.4	41.4	10.8	6.0	6.9	
Parc Hydraulique	PL13	3 536 550	720 200	123	21 Jan 2013	7.2	24.5	7.5	3.2	47.8	14.5	44.4	10.6	6.4	6.6	
Mekhadma	PL25	3 536 230	718 708	129	21 Jan 2013	7.6	27.1	7.9	1.8	48.0	14.5	42.9	6.6	7.4	7.6	
Said Otba	P506	3 535 528	725 075	126	4 Feb 2013	8.3	24.3	8.1	1.7	52.6	14.6	42.8	11.0	7.5	7.8	
Said Otba	P506	3 535 528	725 075	126	1992	6.7	23.3	7.5	1.8	54.4	17.6	33.3	4.1	22.2	5.2	
Mekhadma	P566	3 540 433	719 661	115	27 Jan 2013	9.0	24.6	7.6	1.7	62.5	15.2	71.6	3.0	4.6	6.1	
Mekhadma	PL17	3 536 908	718 511	130	21 Jan 2013	9.4	24.5	8.1	3.4	63.2	15.6	77.2	2.5	4.1	5.1	
Palm. Gara Krima	P413	3 530 116	722 775	130	4 Feb 2013	10.1	30.2	7.9	1.6	63.6	21.5	88.3	4.1	4.2	4.7	
Mekhadma	PL25	3 536 230	718 708	129	1992	9.5	23.7	8.0	0.6	75.6	10.6	10.2	2.6	32.9	9.5	
Said Otba (Bab Sbaa)	P066	3 542 636	718 957	126	1992	7.8	23.5	7.6	1.5	80.2	12.5	45.9	2.5	23.6	5.9	
CEM Malek Bennabi	PL03	3 540 010	725 738	130	1992	7.3	23.9	7.6	3.1	84.1	30.6	108.6	2.2	10.2	9.0	
Entreprise nationale de télévision	PL21	3 536 074	721 268	128	1992	9.7	23.8	7.3	4.5	84.3	23.7	61.6	3.8	33.5	1.9	
Hôtel Transat	PL23	3 538 419	720 950	126	28 Jan 2013	15.0	24.2	8.2	4.5	86.6	16.7	79.9	3.2	14.5	6.9	
Entreprise nationale de télévision	PL21	3 536 074	721 268	128	28 Jan 2013	16.4	25.7	7.5	2.0	99.9	17.4	85.5	5.7	15.7	7.6	
Mekhadma	PL05	3 537 109	718 419	137	21 Jan 2013	16.8	24.8	7.6	2.0	101.3	17.7	85.9	5.9	16.7	7.6	
Beni Thour	PL44	3 536 039	721 673	134	1992	4.7	23.9	7.2	2.7	109.8	67.2	134.7	5.7	42.0	8.8	
Tazegrart	PLSN1	3 537 675	71 9416	125	22 Jan 2013	17.1	24.9	8.0	3.4	114.2	18.1	92.9	12.8	16.9	7.8	
CEM Malek Bennabi	PL03	3 540 010	725 738	130	27 Jan 2013	10.8	23.1	7.5	3.3	117.3	14.7	116.4	2.1	9.0	7.2	
El Bour	P006	3 564 272	719 421	161	3 Feb 2013	18.3	23.6	7.8	6.3	131.9	18.1	96.3	8.6	27.1	8.0	
Aïn Moussa	P015	3 551 711	720 591	103	1992	12.4	23.6	7.7	2.4	134.7	28.2	73.0	3.1	52.4	6.3	
Station de Pompage	PL04	3 541 410	723 501	138	27 Jan 2013	19.0	26.4	7.9	4.0	138.0	16.7	108.8	13.1	19.5	8.7	
Drain Chott Ouargla	D. Ch				1992		23.9	7.7	2.7	142.2	24.5	96.31	3.2	44.2	3.0	
Beni Thour	PL44	3 536 039	721 673	134	28 Jan 2013	20.2	25.8	7.8	5.0	153.0	17.7	125.9	6.3	22.8	8.1	
CNMC (Société nationale des matériaux de construction)	PL27	3 535 474	718 407	126	21 Jan 2013	21.2	24.8	8.1	1.7	169.4	18.4	130.3	4.9	27.8	8.6	
Bamendil	P076	3 540 137	716 721	118	26 Jan 2013	22.3	27.2	7.6	4.3	171.5	17.1	130.8	6.3	28.0	8.8	
N'Goussa	P041	3 559 563	716 543	135	26 Jan 2013	25.9	24.5	8.2	8.0	208.6	13.4	198.9	3.6	11.8	8.8	
N'Goussa	P009	3 559 388	717 707	123	26 Jan 2013	27.5	28.4	8.4	11.5	208.8	15.8	195.1	2.7	18.7	9.0	
	LTP16				1992	11.5	23.8	7.5	3.8	213.4	48.6	147.9	7.5	75.3	4.3	
	P100				1992	17.2	23.6	7.6	3.4	235.0	46.4	264.8	4.7	25.6	5.6	
Chott Adjadja Aven	PLX1	3 540 758	726 115	132	28 Jan 2013	32.9	23.4	8.0	4.4	245.6	20.9	141.4	26.9	44.6	17.7	
Route Frane	P003	3 569 043	721 496	134	2 Feb 2013	31.0	23.5	8.0	6.9	252.7	17.9	208.2	9.4	30.0	10.0	
El Bour–N'Goussa	P007	3 562 236	718 651	129	26 Jan 2013	30.1	28.4	7.8	5.4	254.7	15.5	209.2	10.4	28.8	7.5	
Route Aïn Beïda	PLX2	3 537 323	724 063	127	21 Jan 2013	43.3	25.7	8.1	5.2	262.2	93.0	270.4	15.5	62.8	21.7	
Aïn Moussa	P015	3 551 711	720 591	103	25 Jan 2013	32.0	22.7	8.0	2.9	263.0	15.4	206.9	6.6	32.1	9.9	
Aïn Moussa	P402	3 549 503	721 514	138	25 Jan 2013	60.0	28.7	8.6	7.7	313.2	93.9	442.8	23.3	12.6	10.2	
Route Frane	P001	3 572 148	722 366	127	1992		23.6	8.4	4.0	323.6	58.1	331.4	5.0	49.8	4.0	
Aïn Moussa	P014	3 551 466	719 339	131	1992		23.4	7.3	4.0	337.0	64.3	328.7	5.5	62.4	5.5	

Table 3. Continued.

Locality	Site	Lat.	Long.	Elev.	Date	EC	T	pH	Alk.	Cl^-	SO_4^{2-}	Na^+	K^+	Mg^{2+}	Ca^{2+}	Br^-
		(m)				($mS\,cm^{-1}$)	(°C)		($mmol\,L^{-1}$)							
N'Goussa	P019	3 562 960	717 719	113	2 Feb 2013	60.6	27.8	7.7	6.0	356.2	96.0	432.5	29.8	21.0	26.2	
N'Goussa	P018	3 562 122	716 590	110	26 Jan 2013	61.1	26.2	8.4	6.5	372.4	82.3	347.1	22.6	60.7	26.6	
Aïn Moussa	P014	3 551 466	719 339	131	25 Jan 2013	49.0	25.2	7.9	1.8	399.7	21.1	389.3	2.4	19.0	7.4	
Route Sedrata	P113	3 535 586	714 576	105	3 Feb 2013	62.2	24.8	8.2	6.0	414.8	83.8	362.7	33.3	70.2	26.5	
N'Goussa	P009	3 559 388	717 707	123	1992		23.3	7.8	2.4	426.9	57.8	393.8	9.1	59.1	12.0	
Route Frane	P001	3 572 148	722 366	127	2 Feb 2013	66.2	28.3	7.2	6.5	468.7	101.5	350.3	26.0	116.2	35.3	
Sebkhet Safioune	P031	3 577 804	720 172	120	1992		23.8	7.3	6.3	481.8	43.4	326.8	12.6	94.2	23.6	
Sebkhet Safioune	P031	3 577 804	72 0172	120	2 Feb 2013	76.0	27.9	8.1	5.9	500.3	110.3	470.5	28.7	79.1	35.5	
Route Frane	P002	3 570 523	722 028	108	1992		23.8	7.8	6.3	522.4	183.0	653.8	10.0	104.7	11.0	
Sebkhet Safioune	P030	3 577 253	721 936	130	1992		23.5	7.7	4.4	527.7	123.5	533.8	11.6	106.2	10.7	
Oum Raneb	P012	3 554 089	718 612	114	25 Jan 2013	64.1	30.3	7.8	7.8	534.3	20.9	529.6	6.4	19.7	4.7	
Oum Raneb	P012	3 554 089	718 612	114	1992		23.4	7.5	2.7	539.4	60.6	413.6	5.6	112.8	9.4	
Ank Djemel	P423	3 540 881	723 178	102	31 Jan 2013	90.8	23.5	7.5	6.2	636.5	101.3	495.5	38.3	125.8	30.3	
Said Otba Chott	P096	3 540 265	724 729	111	1992		23.6	7.7	3.7	645.1	78.5	357.3	6.0	208.4	12.9	
Sebkhet Safioune	P030	3 577 253	721 936	130	03/02/2013	64.7	23.1	7.8	3.7	671.8	90.3	742.9	16.0	41.5	7.7	
N'Goussa	P017	3 560 256	715 781	130	26 Jan 2013	100.1	31.0	7.1	3.8	679.3	114.1	597.8	10.7	125.9	26.3	
Ank Djemel	P021	3 573 943	723 161	105	1992		23.6	7.4	4.2	700.8	154.5	605.7	53.6	163.1	14.2	
Station de Pompage	PL04	3 541 410	723 501	138	1992		23.6	7.4	2.4	716.3	34.8	560.1	7.0	99.6	11.0	
Route Frane	P002	3 570 523	722 028	108	2 Feb 2013	62.8	26.9	7.6	1.7	748.5	62.6	651.5	14.7	77.7	27.3	
Said Otba chott	P096	3 540 265	724 729	111	3 Feb 2013	68.3	25.9	8.7	1.2	771.0	53.1	615.9	23.5	69.6	50.4	
N'Goussa	P019	3 562 960	717 719	113	1992		23.3	7.7	2.4	779.1	77.1	711.5	9.2	95.6	12.1	
Said Otba (Bab Sbaa)	P066	3 542 636	718 957	126	3 Feb 2013	150.6	26.2	7.2	12.3	799.1	283.0	1249.7	19.0	37.6	18.1	
Ank Djemel	P021	3 573 943	723 161	105	24 Jan 2013	82.3	29.6	7.6	2.4	800.4	94.4	824.0	11.0	53.4	25.4	
N'Goussa	P018	3 562 122	716 590	110	1992		23.3	7.5	1.2	818.7	81.0	244.2	49.5	319.4	24.8	
Oum Raneb	P162	3 546 133	725 129	98	25 Jan 2013	160.0	30.7	7.2	2.4	842.8	289.9	1309.9	13.3	33.5	17.7	
Route Sedrata	P113	3 535 586	714 576	105	1992		23.7	7.7	2.8	954.9	124.9	997.5	13.3	86.7	11.7	
Oum Raneb	PZ12	3 547 234	722 931	110	5 Feb 2013	114.9	27.4	7.4	2.9	980.1	15.5	930.8	7.5	23.9	14.2	
Hôtel Transat	PL23	3 538 419	720 950	126	1992		23.5	7.4	3.0	1103.3	94.5	707.8	19.1	270.9	13.3	
Sebkhet Safioune	P023	3 577 198	725 726	99	1992		23.3	7.4	2.3	1177.0	91.1	1058.2	11.7	133.5	12.4	
Sebkhet Safioune	P034	3 579 698	725 633	97	5 Feb 2013	130.0	34.9	8.1	1.8	1189.1	14.7	1055.1	18.3	56.4	17.4	
Sebkhet Safioune	P023	3 577 198	725 726	99	5 Feb 2013	117.9	29.4	8.2	1.9	1209.3	15.6	1129.4	8.4	42.9	10.2	
Chott Adjadja	PLX1	3 540 758	726 115	132	1992		23.6	8.0	3.8	1296.7	134.0	1458.7	5.2	48.0	4.3	
Sebkhet Safioune	P063	3 545 586	725 667	99	1992		23.5	7.5	1.9	1379.4	139.6	1257.4	18.6	182.3	10.0	
	LTP06				1992		23.8	7.6	7.8	1638.7	712.1	2621.6	41.6	190.5	13.3	
Bamendil	P076	3 540 137	716 721	118	1992		23.5	7.7	5.7	1743.6	143.4	1321.9	26.9	331.4	12.3	
El Bour–N'Goussa	P007	3 562 236	718 651	129	1992		23.3	7.7	1.4	1860.5	91.6	1434.7	26.2	278.8	13.3	
Sebkhet Safioune	P063	3 545 586	725667	99	5 Feb 2013	178.9	26.7	7.7	1.4	1887.9	92.9	1455.8	26.7	282.9	13.4	
	P044				1992		23.4	7.8	4.5	2106.1	18.3	1765.5	27.3	171.2	6.5	
	P093				1992		23.6	7.5	1.5	2198.6	182.1	1957.5	29.5	278.2	10.4	
	P042				1992		23.4	7.6	1.1	2330.9	101.2	1963.7	52.2	248.1	11.2	
	P068				1992		23.5	7.5	3.4	2335.7	222.1	2302.3	26.8	219.9	7.2	

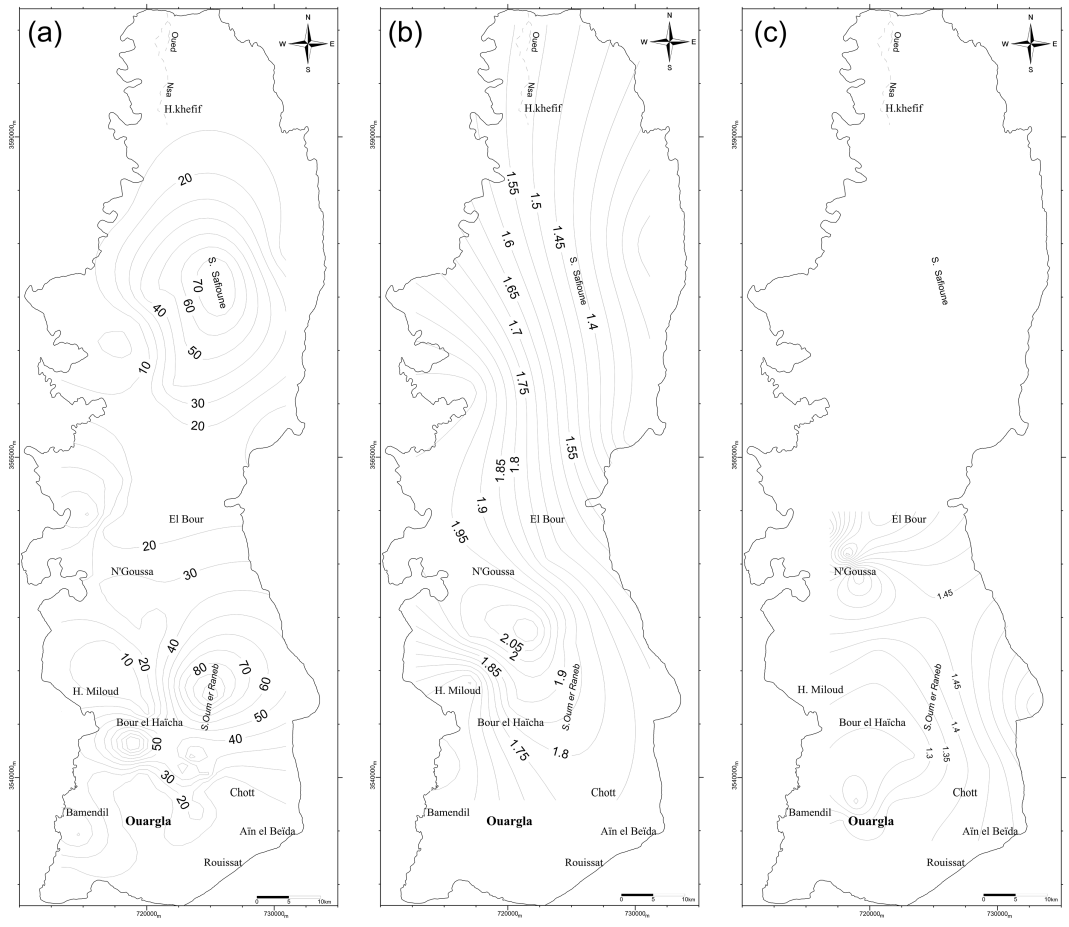

Figure 5. Contour maps of the salinity (expressed as global mineralization) in the aquifer system of the **(a)** phreatic aquifer and **(b, c)** Complexe Terminal (with **b** indicating Mio-Pliocene and **c** indicating Senonian); figures are isovalues of global mineralization (values in $g\,L^{-1}$).

Average values of mixing fractions from each aquifer to the phreatic waters computed by means of Eq. (2) gave the rates of 65 % for the CI aquifer and 35 % for the CT aquifer.

A mixture of a phreatic water component that is close to cluster I (i.e., P433) with another component which is rather close to cluster II (i.e., P039) (Figs. 13 and 14), for an intermediate water with a $\delta^{18}O$ signature ranging from -5 to -2 ‰, gives mixture fraction values of 52 % for cluster I and 48 % for cluster II. Isotope results will be used to independently cross-check the validity of the mixing fractions derived from an inverse modeling involving chemical data (see Sect. 3.6).

Turonian evaporites are found to lie in between the CI deep aquifer and the Senonian and Miocene formations bearing the CT aquifer. CT waters can thus simply originate from ascending CI waters that dissolve Turonian evaporites, a process which does not involve any change in ^{18}O content. Conversely, phreatic waters result, to a minor degree, from evaporation and mostly from dissolution of sabkha evaporites by ^{18}O-enriched rainwater and mixing with CI/CT waters.

Tritium content of water

Tritium contents of the Phr aquifer are relatively small (Table 4), they vary between 0 and 8 TU. Piezometers PZ12, P036 and P068 show values close to 8 TU; piezometers P018, P019, P416, P034, P042 and P093 exhibit values ranging between 5 and 6 TU; and the rest of the samples' concentrations are lower than 2 TU.

These values are dated back to November 1992, so they are old values and they are considered high comparatively to what is expected to be found nowadays. In fact, at present times, tritium figures have fallen lower than 5 TU in precipitation measured in the northern part of the country.

Tritium content of precipitation was measured as 16 TU in 1992 on a single sample that was collected from the National Agency for Water Resources station in Ouargla. A major part of this rainfall evaporates back into the atmosphere that is unsaturated in moisture. Consequently, enrichment in tritium happens as water evaporates back. The lightest fractions (isotopes) are the ones that escape first, enriching the remaining fraction in tritium. The 16 TU value would thus

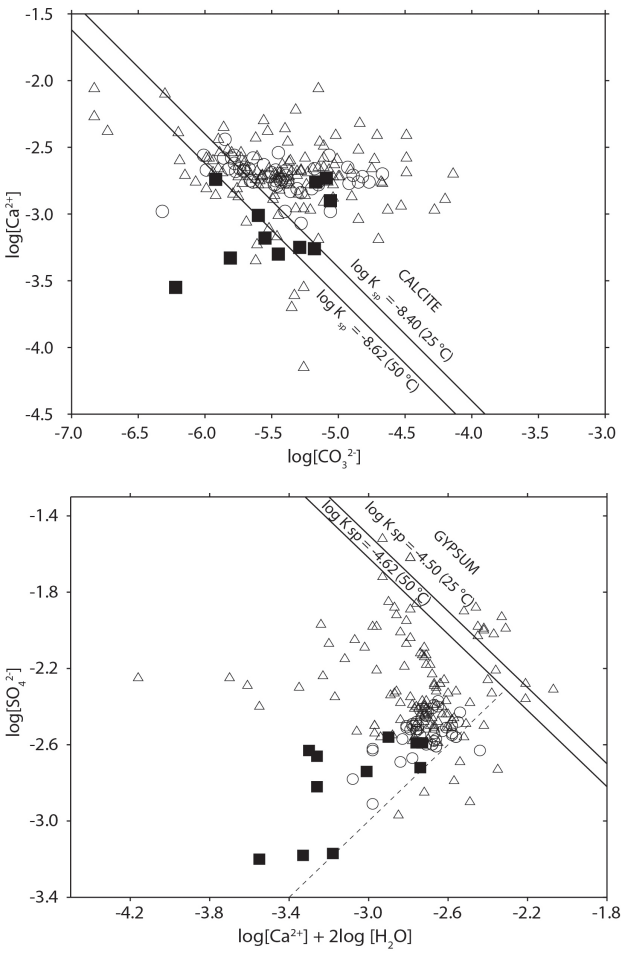

Figure 6. Equilibrium diagrams of calcite (top panel) and gypsum (bottom panel) for the Continental Intercalaire (filled squares), Complexe Terminal (open circles) and phreatic (open triangles) aquifers. Equilibrium lines are defined as $\log\{Ca^{2+}\} + \log\{CO_3^{2-}\} = \log K_{sp}$ for calcite and $\log\{Ca^{2+}\} + 2\log\{H_2O\} + \log\{SO_4^{2-}\} = \log K_{sp}$ for gypsum.

correspond to a rainy event that had happened during the field campaign (5 and 6 November 1992). It is the most representative value for that region and for that time. Unfortunately, all the other stations (Algiers, Ankara and Tenerife) (Martinelli et al., 2014) are subject to a completely different climatic regime and (besides the fact that they have more recent values) can absolutely not be used for our case. Therefore, all the assumptions based on recent tritium rain values do not apply to this study.

Depleted contents in ^{18}O and low tritium concentrations for phreatic waters fit the mixing scheme well and confirm the contribution from the older and deeper CI/CT groundwaters. The affected areas were clearly identified in the field and correspond to locations that are subject to a recycling and a return of irrigation waters whose origin are CI/CT boreholes. Moreover, the mixing that is clearly brought to light by

Table 3. Continued.

Locality	Site	Lat.	Long.	Elev.	Date	EC	T	pH	Alk.	Cl^-	SO_4^{2-}	Na^+	K^+	Mg^{2+}	Ca^{2+}	Br^-
		(m)				($mS\,cm^{-1}$)	(°C)		($mmol\,L^{-1}$)							
Oum Raneb	PZ12	3 547 234	722 931	110	1992		23.3	7.6	2.2	2405.6	109.9	2178.6	25.2	199.4	12.7	
Hassi Debiche	P416	3 581 097	730 922	106	1992		23.3	7.8	4.3	2433.7	178.9	2361.1	24.3	196.1	9.2	
N'Goussa	P041	3 559 563	716 543	135	1992		23.4	7.9	2.1	2599.7	324.6	2879.0	44.6	152.8	11.0	
Sebkhet Safioune	P034	3 579 698	725 633	97	1992		23.3	7.8	1.9	2752.0	134.1	2616.8	24.4	180.1	10.5	
	P039				1992		23.4	6.9	1.9	4189.5	201.4	4042.6	17.9	257.8	9.2	
Sebkhet Safioune	P074				1992		23.5	6.5	4.2	4356.5	180.9	2759.9	57.4	930.1	22.6	
Sebkhet Safioune	P037				1992		23.4	6.9	1.5	4953.8	184.5	4611.1	2.9	347.6	7.9	
Sebkhet Safioune	P036				1992		23.4	7.5	1.4	4972.8	108.1	4692.2	36.8	221.1	9.6	

For longitude and latitude, the reference is UTM 31 projection for north Sahara 1959 (CLARKE 1880 ellipsoid).

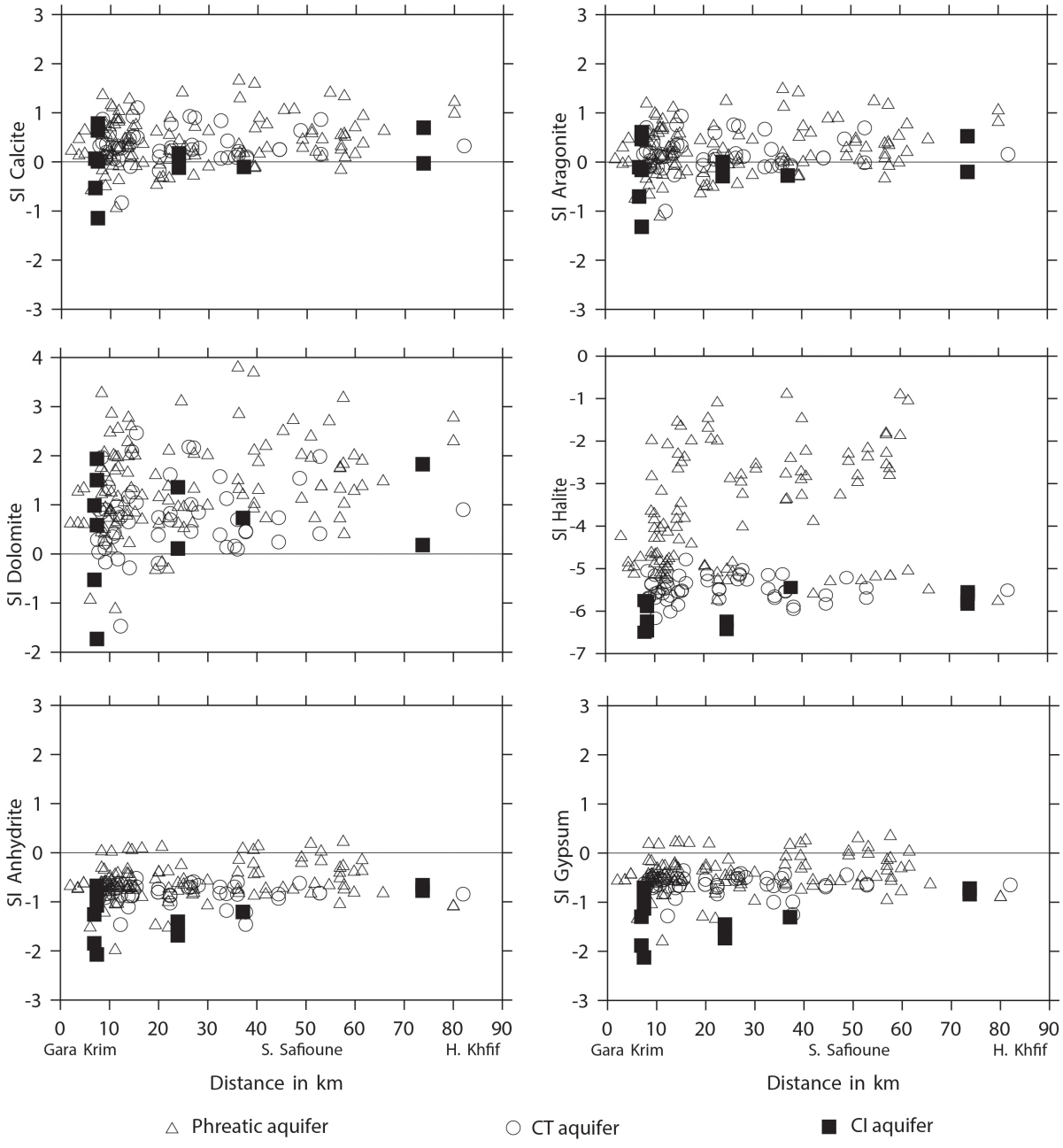

Figure 7. Variation of saturation indices with distance from south to north in the region of Ouargla.

the Cl^- versus ^{18}O diagrams (Figs. 13 and 14) could partly derive from an ascending drainage from the deep and confined CI aquifer (exhibiting depleted homogenous ^{18}O contents and very low tritium), a vertical leakage that is favored by the Amguid El Biod highly faulted area (Guendouz and Moulla, 1996; Edmunds et al., 2003; Guendouz et al., 2003; Moulla et al., 2012).

3.6 Inverse modeling

We assume that the relationship between ^{18}O and Cl^- data obtained in 1992 is stable with time, which is a logical assumption as times of transfer from CI to both CT and Phr are very long. Considering both ^{18}O and Cl^- data, CI, CT and Phr data populations can be categorized. The CI and CT do not show appreciable ^{18}O variations and can be considered as a single population. The Phr samples consist, however, of different populations: cluster I, with $\delta^{18}O$ values close to -8 and small Cl^- concentrations, more specifically less

Table 4. Isotopic data ^{18}O and ^{3}H and chloride concentration in the Continental Intercalaire, Complexe Terminal and phreatic aquifers (sampling campaign in 1992).

Piezometer	Cl^- (mmol L^{-1})	$\delta^{18}O$ (‰)	^{3}H (UT)	Piezometer	Cl^- (mmol L^{-1})	$\delta^{18}O$ (‰)	^{3}H (UT)	Piezometer	Cl^- (mmol L^{-1})	$\delta^{18}O$ (‰)	^{3}H (UT)
Phreatic aquifer											
P007	1860.5	−2.5	0	PL15	23.5	−7.85	0.6(1)	P074	4356.4	3.4	6.8(8)
P009	426.9	−6.6	1.2(3)	P066	80.2	−8.1	0.8(1)	PL06	14.2	−8.1	1.0(2)
P506	54.4	−6.8	1.6(3)	PL23	1103.3	−6.1	0	PL30	24.3	−7.48	2.4(4)
P018	818.7	−2.9	6.2(11)	P063	1379.3	−3.4	8.7(15)	P002	522.4	−5.7	0.6(1)
P019	779.1	−4.7	5.6(9)	P068	2335.6	−3.1	8.8(14)	PL21	84.3	−7.7	1.2(2)
PZ12	2405.5	−2.3	8.1(13)	P030	527.7	−6.6	2.4(4)	PL31	18.9	−7.4	1.6(3)
P023	1176.9	−2.6	0.2(1)	P076	1743.5	−5.6	2.8(5)	P433	12.0	−8.8	0
P416	2433.7	−7.9	5.9(9)	P021	700.7	−5.2	2.6(4)	PL03	84.1	−7.4	1.7(3)
P034	2752.0	−1.8	5.7(9)	PL04	716.3	−2.9		PL44	109.8	−8.8	1.0(2)
P036	4972.7	3.3	2.1(4)	P093	2198.5	−2.6	5.1(8)	PL05	30.9	−7.4	1.9(3)
P037	4953.8	3.1	1.8(3)	P096	645.1	−6.1	4.8(8)	P408	24.2	−7.9	0
P039	4189.5	1.0	2.2(4)	PLX1	1296.6	−5.6	1.1(2)	P116	31.9	−7.2	1.1(2)
P041	2599.7	−0.6	7.3(13)	PLX2	25.7	−7.6	1.3(2)	LTP 16	213.4	−7.5	1.6(3)
P044	2106.1	−4.5	2.7(5)	P015	134.7	−6.8	3.0(5)	P117	32.8	−6.9	0.1
P014	336.9	−6.9	2.8(5)	P001	323.6	−4.7	2.5(4)	PL10	35.0	−7.3	0.2(1)
P012	539.3	−6.4	2.2(4)	P100	235.0	−5.8	0	PL25	75.6	−7.4	0.9(2)
P042	2330.8	2.1	6.0(10)	P056	42.1	−7.0	2.9(5)	LTP30	18.2	−7.5	1.1(2)
P006	19.0	−6.6	0.5(1)	P113	954.9	−4.8	0.8(2)	LTP06	1638.6	−1.9	2.8(5)
P057	28.2	−7.3	1.1(2)	PLX4	31.5	−7.1	0.3(1)	P031	481.8	−6.1	3.0(5)
P059	20.8	−7.8	0	P115	28.8	−2.5	6.8(12)				
Borehole	Cl^- (mmol L^{-1})	$\delta^{18}O$ (‰)	^{3}H (UT)	Borehole	Cl^- (mmol L^{-1})	$\delta^{18}O$ (‰)	^{3}H (UT)	Borehole	Cl^- (mmol L^{-1})	$\delta^{18}O$ (‰)	^{3}H (UT)
Complexe Terminal aquifer											
D5F80	42.2	−7.9		D1F138	28.9	−8.1	0.7(1)	D2F71	13.5	−8.2	0.6(1)
D3F8	29.8	−8.1	1.4(2)	D3F18	21.7	−8.2	0.2(1)	D7F4	10.6	−8.3	0.1(1)
D3F26	34.7	−8.0	0.8(1)	D3F10	14.3	−7.9	1.5(2)	D2F66	11.0	−8.3	
D4F94	20.1	−8.2	0.6(1)	D6F51	28.4	−7.9	0.7(1)	D1F151	10.8	−8.3	0.4(1)
D6F67	18.8	−8.2	3.7(6)	D1F135	18.1	−8.1	1.1(2)	D6F64	11.4	−8.3	4.3(7)
Continental Intercalaire aquifer											
Hadeb I	5.8	−8.0	0	Hadeb II	6.2	−7.9	0.1(1)	Aouinet Moussa	6.5	−7.9	1.1(2)

than 35 mmol L^{-1}; cluster II, with $\delta^{18}O$ values larger than 3 and very large Cl^- concentrations, more specifically larger than 4000 mmol L^{-1} (Table 5); intermediate Phr samples resulting from mixing between clusters I and II (mixing line in Fig. 13, mixing curve in Fig. 14) and from evaporation of cluster I (evaporation line in Fig. 14). The mass-balance modeling has shown that relatively few phases are required to derive observed changes in water chemistry and to account for the hydrochemical evolution in Ouargla's region. The mineral phases' selection is based upon geological descriptions and analysis of rocks and sediments from the area (OSS, 2003; Hamdi-Aïssa et al., 2004).

The inverse model was constrained so that mineral phases from evaporites including gypsum, halite, mirabilite, glauberite, sylvite and bloedite were set to dissolve until they reach saturation, and calcite and dolomite were set to precipitate once they reached saturation. Cation exchange reactions of Ca^{2+}, Mg^{2+}, K^+ and Na^+ on exchange sites were included in the model to check which cations are adsorbed or desorbed during the process. Dissolution and desorption contribute as positive terms in the mass balance, as elements are released in solution. On the other hand, precipitation and adsorption contribute as negative terms, while elements are removed from the solution. $CO_{2_{(g)}}$ dissolution is considered by PHREEQC as a dissolution of a mineral, whereas $CO_{2_{(g)}}$ degassing is dealt with as if it were a mineral precipitation.

Inverse modeling leads to a quantitative assessment of the different solutes' acquisition processes and a mass balance for the salts that are dissolved or precipitated from CI, CT and Phr groundwaters (Fig. 14, Table 6), as follows:

- Transition from CI to CT involves gypsum, halite and sylvite dissolution, and some ion exchange, namely calcium and potassium fixation on exchange sites against magnesium release, with a very small and quite negligible amount of $CO_{2_{(g)}}$ degassing. The maximum elemental concentration fractional error equals 1 %. The

Table 5. Statistical parameters for the Continental Intercalaire (CI), Complexe Terminal (CT) and phreatic (Phr) aquifer samples selected on the basis of $\delta^{18}O$ and Cl^- data (see text).

Aquifer	Size	Parameter	EC ($mS\,cm^{-1}$)	T (°C)	pH	Alk.	Cl^-	SO_4^{2-}	Na^+ ($mmol\,L^{-1}$)	K^+	Mg^{2+}	Ca^{2+}
CI	11	Average	2.2	49.0	7.5	2.3	11.0	4.7	10.3	0.5	3.6	2.4
CI	11	SD	0.3	2.0	0.2	1.0	4.6	2.5	4.6	0.2	2.0	1.8
CT	50	Average	3.2	23.0	7.8	2.3	20.0	8.9	17.0	1.0	5.5	5.6
CT	50	SD	1.1	2.4	0.4	0.8	7.0	2.6	6.0	0.8	2.2	1.7
Phr cluster I	30	Average	3.9	24.0	7.9	2.3	24.7	11.8	24.2	2.1	7.2	5.3
Phr cluster I	30	SD	1.3	1.3	0.4	1.0	6.9	3.4	11.0	1.7	5.0	2.7
Phr cluster II	3	Average		23.4	7.0	2.4	4761.0	158.0	4021.0	32.4	500.0	13.0
Phr cluster II	3	SD		0.1	0.5	1.6	350.0	43.0	1093.0	28.0	378.0	8.0

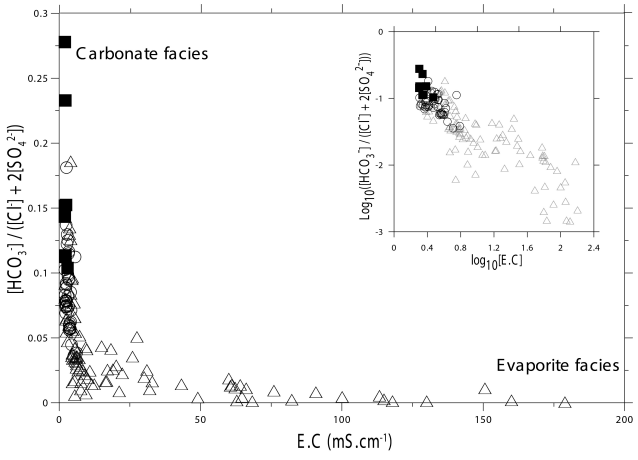

Figure 8. Change from carbonate facies to evaporite from the Continental Intercalaire (filled squares), Complexe Terminal (open circles) and phreatic (open triangles) aquifers.

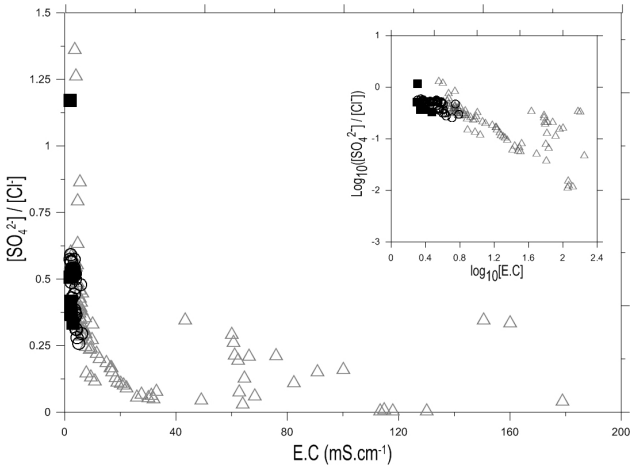

Figure 9. Change from sulfate facies to chloride from the Continental Intercalaire (filled squares), Complexe Terminal (open circles) and phreatic (open triangles) aquifers.

model consists of a minimum number of phases (i.e., six solid phases and $CO_{2(g)}$); another model also implies dolomite precipitation with the same fractional error.

– Transition from CT to an average water component of cluster I involves dissolution of halite, sylvite and bloedite from Turonian evaporites, with a very tiny calcite precipitation. The maximum fractional error in elemental concentration is 4 %. Another model implies $CO_{2(g)}$ escape from the solution, with the same fractional error. Large amounts of Mg^{2+} and SO_4^{2-} are released within the solution (Sharif et al., 2008; Li et al., 2010; Carucci et al., 2012).

– The formation of Phr cluster II can be modeled as being a direct dissolution of salts from the sabkha by rainwater with positive $\delta^{18}O$; the most concentrated water (P036 from Sebkhet Safioune) is taken here for cluster II, and pure water is taken as rainwater. In a descending order of amount, halite, sylvite, gypsum and huntite are the minerals that are the most involved in the dissolution process. A small amount of calcite precipitates while some Mg^{2+} is released versus K^+ fixation on exchange sites. The maximum elemental fractional error in the concentration is equal to 0.004 %. Another model implies dolomite precipitation with some more huntite dissolving, instead of calcite precipitation, but salt dissolution and ion exchange are the same. Huntite, dolomite and calcite stoichiometries are linearly related, so both models can fit field data, but calcite precipitation is preferred compared to dolomite precipitation at low temperature.

– The origin of all phreatic waters can be explained by a mixing in variable proportions of cluster I and cluster II. For instance, waters from cluster I and cluster II can easily be separated by their $\delta^{18}O$, respectively, close to

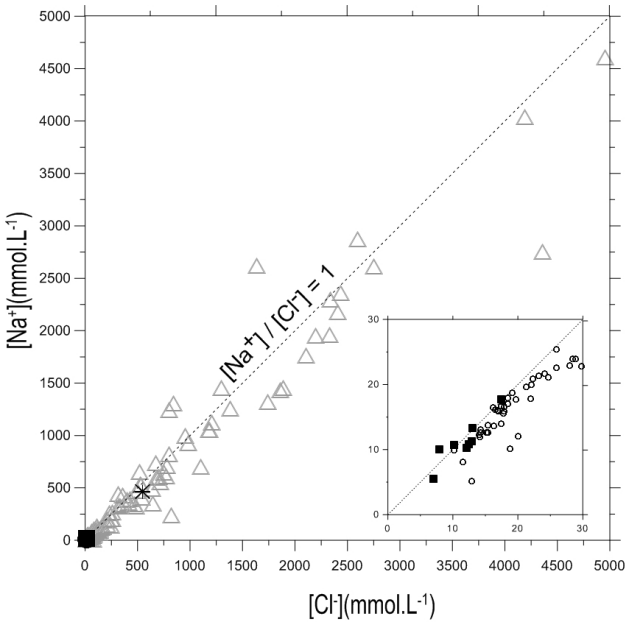

Figure 10. Correlation between Na^+ and Cl^- concentrations in the Continental Intercalaire (filled squares), Complexe Terminal (open circles) and phreatic (open triangles) aquifers. Seawater composition (star) is $[Na^+] = 459.3\,\text{mmol}\,L^{-1}$ and $[Cl^-] = 535.3\,\text{mmol}\,L^{-1}$ (Stumm and Morgan, 1999, p. 899).

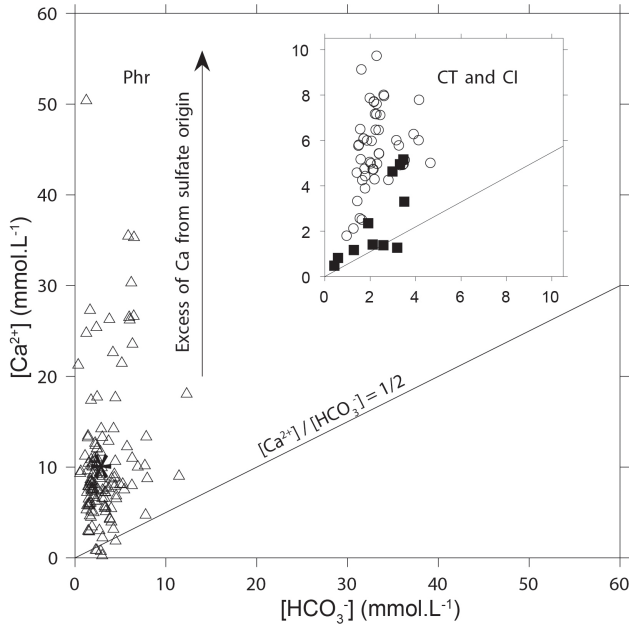

Figure 11. Calcium versus HCO_3^- diagram in the Continental Intercalaire (filled squares), Complexe Terminal (open circles) and phreatic (open triangles) aquifers. Seawater composition (star) is $[Ca^{2+}] = 10.2\,\text{mmol}\,L^{-1}$ and $[HCO_3^-] = 2.38\,\text{mmol}\,L^{-1}$ (Stumm and Morgan, 1999, p. 899).

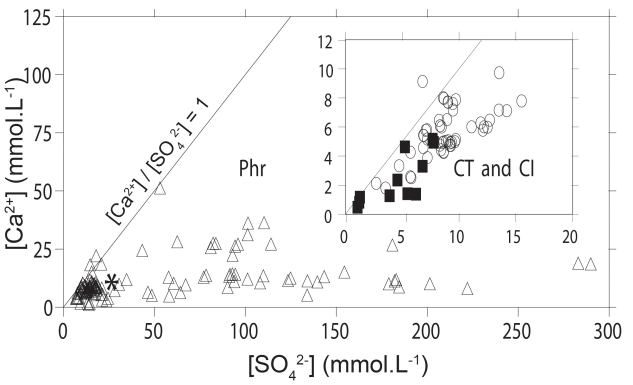

Figure 12. Calcium versus SO_4^{2-} diagram in the Continental Intercalaire (filled squares), Complexe Terminal (open circles) and phreatic (open triangles) aquifers. Seawater composition (star) is $[Ca^{2+}] = 10.2\,\text{mmol}\,L^{-1}$ and $[SO_4^{2-}] = 28.2\,\text{mmol}\,L^{-1}$ (Stumm and Morgan, 1999, p. 899).

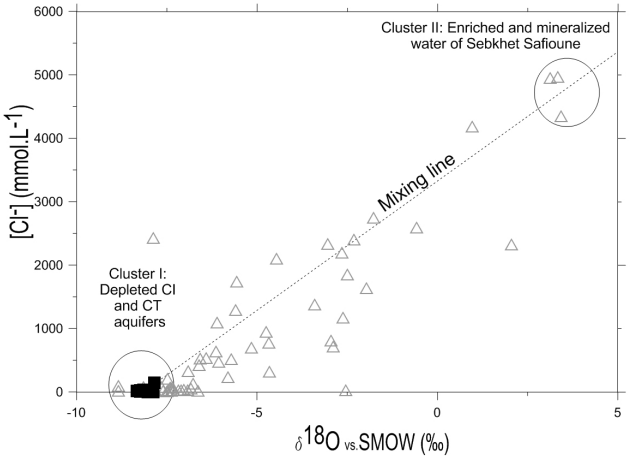

Figure 13. Chloride concentration versus $\delta^{18}O$ in the Continental Intercalaire (filled squares), Complexe Terminal (open circles) and phreatic (open triangles) aquifers from Ouargla.

−8 and +3.5 ‰ (Figs. 13 and 14). Mixing the two clusters is of course not an inert reaction, but rather results in the dissolution and the precipitation of minerals. Inverse modeling is then used to compute both mixing rates and the extent of matter exchange between soil and solution. For example, a phreatic water (piezometer P068) with intermediate values ($\delta^{18}O = -3$ and $[Cl^-] \simeq 2$ M) is explained by the mixing of 58 % water from cluster I and 42 % from cluster II. In addition, calcite precipitates, Mg^{2+} fixes on exchange sites against Na^+ and K^+, and gypsum dissolves, as does a minor amount of huntite (Table 6). The maximum elemental concentration fractional error is 2.5 % and the mixing fractions' weighted $\delta^{18}O$ is −3.17 ‰, which is very close to the measured value (−3.04 ‰). All the other models, making use of a minimum number of phases, and not taking into consid-

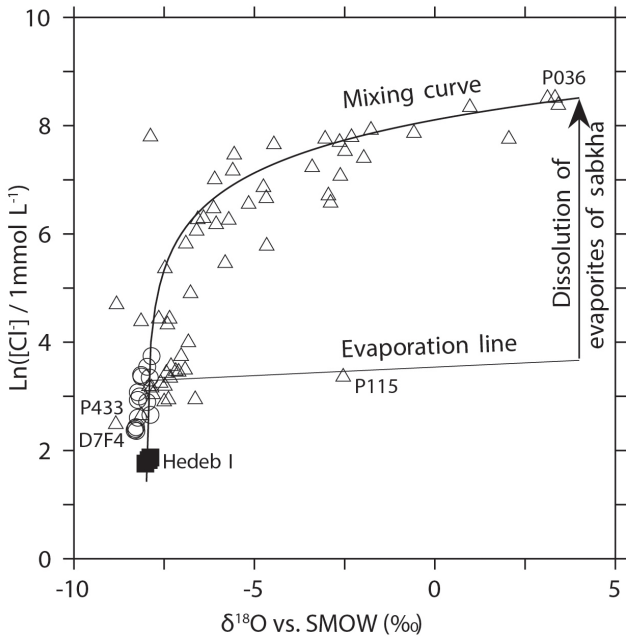

Figure 14. Log [Cl^-] concentration versus $\delta^{18}O$ in Continental Intercalaire (filled squares), Complexe Terminal (open circles) and phreatic (open triangles) aquifers from Ouargla.

eration ion exchange reactions are not found compatible with isotope data. Mixing rates obtained with such models are, for example, 98 % of cluster I and 0.9 % of cluster II, which leads to a $\delta^{18}O = (-7.80‰)$ which is quite far from the real measured value ($-3.04‰$).

The main types of groundwaters occurring in the Ouargla basin are thus explained and could quantitatively be reconstructed. An exception is, however, sample P115, which is located exactly on the evaporation line of Phr cluster I. Despite numerous attempts, it could not be quantitatively rebuilt. Its ^3H value (6.8) indicates that it is derived from a more or less recent water component with very small salt content, most possibly affected by rainwater and some preferential flow within the piezometer. As this is the only sample on this evaporation line, there remains doubt regarding its significance.

Globally, the summary of mass transfer reactions occurring in the studied system (Table 6) shows that gypsum dissolution results in calcite precipitation and $CO_{2_{(g)}}$ dissolution, thus acting as an inorganic carbon sink.

4 Conclusions

Two of the aquifers studied in this work, Complexe Terminal and Continental Intercalaire, are the main aquifers of Sahara, by extent (thousands of kilometers from the recharge area to the Gulf of Gabès) and time of transfer (thousands of years). The last one, the phreatic aquifer, is a shallow aquifer. The chemical facies of these aquifers have long been qualitatively described. Our results quantitatively explain, for the first time, the processes that occur during upward leakage through interaction between solution and the mineral constituents of the aquifers and ultimately by mixing with surface waters. The hydrochemical study of the aquifer system occurring in Ouargla's basin allowed us to identify the origin of its mineralization. Waters exhibit two different facies: sodium chloride and sodium sulfate for the phreatic aquifer (Phr), sodium sulfate for the Complexe Terminal (CT) aquifer and sodium chloride for the Continental Intercalaire (CI) aquifer. Calcium carbonate precipitation and evaporite dissolution explain the facies change from carbonate to sodium chloride or sodium sulfate that is recorded. However, reactions imply many minerals with common ions, deep reactions without evaporation, as well as shallow processes affected by both evaporation and mixing. Those processes are separated by considering both chemical and isotopic data, and quantitatively explained making use of an inverse geochemical modeling. The latter was applied, for the first time ever, in Algeria, to an extreme environment featuring a lack of data on a scarce natural resource such as Saharan groundwater. The populations of the region rely on this resource for their daily drinkable water as well as for agriculture, which mainly consists of date production and some vegetables that grow within the date-palm groves. Results obtained through inverse modeling could help water resources managers, both at the local and the regional scales, to gather the necessary information for an integrated management of that vital resource. Moreover, and regarding the large geographic scale of the aquifers, such a pilot study could be taken as a supporting work to further investigations elsewhere in similar regions. The present study leads to the main result that phreatic waters do not originate simply from infiltration of rainwater and dissolution of salts from the sabkhas. Conversely, Phr waters are largely influenced by the upwardly mobile deep CT and CI groundwaters, with fractions of the latter interacting with evaporites from the Turonian formations. Phreatic water occurrence is explained as a mixture of two end-member components: cluster I, which is very close to CI and CT, and cluster II, which is highly mineralized and results from the dissolution by rainwater of salts from the sabkhas. At depth, CI leaks upwardly and dissolves gypsum, halite and sylvite, with some ion exchange, to give waters of the CT aquifer composition. CT transformation into Phr cluster I waters involves the dissolution of Turonian evaporites (halite, sylvite and bloedite) with minor calcite precipitation. At the surface, direct dissolution by rainwater of salts from sabkhas (halite, sylvite, gypsum and some huntite) with precipitation of calcite and Mg^{2+}/K^+ ion exchange results in cluster II Phr composition. All phreatic groundwaters result from a mixing of cluster I and cluster II water that is accompanied by calcite precipitation, fixation of Mg^{2+} on ion exchange sites against the release of K^+ and Na^+. Moreover, some $CO_{2_{(g)}}$ escapes from the solution at depth, but dissolves much more at the surface.

Table 6. Summary of mass transfer for geochemical inverse modeling. Phases and thermodynamic database are from PHREEQC 3.0 (Parkhurst and Appelo, 2013).

Phases	Stoichiometry	CI/CT	CT/Phr I	Rainwater/P036	PhrI/PhrII 60/40 %
Calcite	$CaCO_3$	–	-6.62×10^{-6}	-1.88×10^{-1}	-2.26×10^{-1}
$CO_{2_{(g)}}$	CO_2	-6.88×10^{-5}	–	8.42×10^{-4}	5.77×10^{-4}
Gypsum	$CaSO_4 \cdot 2H_2O$	4.33×10^{-3}	–	1.55×10^{-1}	1.67×10^{-1}
Halite	NaCl	7.05×10^{-3}	3.76×10^{-3}	6.72×10^{0}	1.28×10^{0}
Sylvite	KCl	2.18×10^{-3}	1.08×10^{-3}	4.02×10^{-1}	–
Bloedite	$Na_2Mg(SO_4)_2 \cdot 4H_2O$	–	1.44×10^{-3}	–	–
Huntite	$CaMg_3(CO_3)_4$	–	–	4.74×10^{-2}	5.65×10^{-2}
Ca ion exchange	CaX_2	-1.11×10^{-3}	–	–	–
Mg ion exchange	MgX_2	1.96×10^{-3}	–	1.75×10^{-1}	-2.02×10^{-1}
Na ion exchange	NaX	–	–	–	3.92×10^{-1}
K ion exchange	KX	-1.69×10^{-3}	–	-3.49×10^{-1}	1.20×10^{-2}

Values are in mol kg^{-1} H_2O. Positive-phase (mass entering solution) and negative-phase (mass leaving solution) mole transfers indicate dissolution and precipitation, respectively; this indicates no mass transfer.

The most complex phenomena occur during the dissolution of Turonian evaporites while CI leaks upwardly towards CT, and from Phr I to Phr II, while the transition from CT to Phr I implies a very limited number of phases. Globally, gypsum dissolution and calcite precipitation processes both act as an inorganic carbon sink.

5 Data availability

The Supplement related to this article is available online at doi:10.5281/zenodo.32287.

Appendix A

According to a simple Rayleigh equation, the evolution of the heavy isotope ratio in the remaining liquid R_l is given by

$$R_l \approx R_{l,0} \times f_l^{\alpha-1}, \tag{A1}$$

where f_l is the fraction of remaining liquid and α the fractionation factor.

The fraction of remaining liquid is derived from chloride concentration, as chloride can be considered conservative during evaporation: all phreatic waters are undersaturated with respect to halite, which precipitates only in the last stage. Hence, the following equation holds:

$$f_l \equiv \frac{n_{w,1}}{n_{w,0}} = \frac{\left[Cl^-\right]_0}{\left[Cl^-\right]_1}. \tag{A2}$$

By taking natural logarithms, one obtains

$$\ln R_l \approx (1-\alpha) \times \ln\left[Cl^-\right] + \text{constant}. \tag{A3}$$

As, by definition,

$$R_l \equiv R_{SD} \times \left(1 + \frac{\delta^{18}O}{1000}\right), \tag{A4}$$

one has

$$\begin{aligned} \ln R_l &\equiv \ln R_{SD} + \ln\left(1 + \frac{\delta^{18}O}{1000}\right), \\ &\approx \ln R_{SD} + \frac{\delta^{18}O}{1000}. \end{aligned} \tag{A5}$$

Hence, with base 10 logarithms,

$$\begin{aligned} \delta^{18}O &\approx 1000(1-\alpha)\log\left[Cl^-\right] + \text{constant}, \\ &\approx -\epsilon \log\left[Cl^-\right] + k, \end{aligned} \tag{A6}$$

where, as classically defined, $\epsilon = 1000(\alpha - 1)$ is the enrichment factor.

Competing interests. The authors declare that they have no conflict of interest.

Acknowledgements. The authors wish to thank the staff members of the National Agency for Water Resources in Ouargla (ANRH) and the Laboratory of Algerian Waters (ADE) for the support provided to the Technical Cooperation programme within which this work was carried out. Analyses of ^{18}O were funded by the project CDTN/DDHI (Guendouz and Moulla, 1996). The support of University of Ouargla and of INRA for travel grants of R. Slimani and G. Bourrié are gratefully acknowledged too.

Edited by: M. Giudici
Reviewed by: G. Martinelli and one anonymous referee

References

ANRH: Inventaire des forages de la Wilaya de Ouargla, Rapport technique, Agence Nationale des Ressources Hydrauliques, Direction régionale Sud, Ouargla, 2011.

Aumassip, G., Dagorne, A., Estorges, P., Leèvre-Witier, P., Mahrour, F., Nesson, C., Rouvillois-Brigol, M., and Trecolle, G.: Aperçus sur l'Évolution du paysage quaternaire et le peuplement de la région de Ouargla, Libyca, Cnrpah, Tome XX, Algérie, 205–257, 1972.

Belkhiri, L., Boudoukha, A., Mouni, L., and Baouz, T.: Application of multivariate statistical methods and inverse geochemical modeling for characterization of groundwater – A case study: Ain Azel plain (Algeria), Geoderma, 159, 390–398, 2010.

Belkhiri, L., Mouni, L., and Boudoukha, A.: Geochemical evolution of groundwater in an alluvial aquifer: Case of El Eulma aquifer, East Algeria, J. Afr. Earth Sci., 66–67, 46–55, 2012.

Carucci, V., Petitta, M., and Aravena, R.: Interaction between shallow and deep aquifers in the Tivoli Plain (Central Italy) enhanced by groundwater extraction: A multi-isotope approach and geochemical modeling, Appl. Geochem., 27, 266–280, doi:10.1016/j.apgeochem.2011.11.007, 2012.

Charlton, S., Macklin, C., and Parkhurst, D.: PhreeqcI – A graphical user interface for the geochemical computer program PHREEQC, Rapport technique, US Geological Survey Water-Resources, USA, 1996.

Chellat, S., Bourefis, A., Hamdi-Aïss, a. B., and Djerrab, A.: Paleoenvironemental reconstitution of Mio-pliocenes sandstones of the lower-Sahara at the base of exoscopic and sequential analysis, Pensee J., 76, 34–51, 2014.

Chkir, N., Guendouz, A., Zouari, K., Hadj Ammar, F., and Moulla, A.: Uranium isotopes in groundwater from the continental intercalaire aquifer in Algerian Tunisian Sahara (Northern Africa), J. Environ. Radioact., 100, 649–656, doi:10.1016/j.jenvrad.2009.05.009, 2009.

Cornet, A. and Gouscov, N.: Les eaux du Crétacé inférieur continental dans le Sahara algérien: nappe dite "Albien", in: Congrès géologique international, vol. tome II, Alger, p. 30, 1952.

Dai, Z., Samper, J., and Ritzi, R.: Identifying Geochemical Processes By Inverse Modeling of Multicomponent Reactive Transport in the Aquia Aquifer, Geosphere, 2, 210–219, 2006.

Deutsch, W.: Groundwater Chemistry-Fundamentals and Applications to Contamination, Lewis Publishers, New York, 1997.

Dubief, J.: Essai sur l'hydrologie superficielle au Sahara, Direction du service de la colonisation et de l'hydraulique, Service des Études scientifiques, Algérie, 1953.

Dubief, J.: Le climat du Sahara, Hors-série, Institut de recherches sahariennes, Algérie, 1963.

Eckstein, G. and Eckstein, Y.: A hydrogeological approach to transboundary ground water resources and international law, Am. Univers. Int. Law Rev., 19, 201–258, 2003.

Edmunds, W., Guendouz, A., Mamou, A., Moulla, A., Shand, P., and Zouari, K.: Groundwater evolution in the continental intercalaire aquifer of southern Algeria and Tunisia: trace element and isotopic indicators, Appl. Geochem., 18, 805–822, 2003.

Fontes, J., Yousfi, M., and Allison, G.: Estimation of long-term, diffuse groundwater discharge in the northern Sahara using stable isotope profiles in soil water, J. Hydrol., 86, 315–327, 1986.

Foster, S., Margat, J., and Droubi, A.: Concept and importance of nonrenewable resources, no. 10 in IHP-VI Series on Groundwater, UNESCO, Paris, 2006.

Furon, R.: Géologie de l'Afrique, 2nd Edn., Payot, Paris, 1960.

Gonfiantini, R., Conrad, G., Fontes, J.-C., Sauzay, G., and Payne, B.: Étude isotopique de la nappe du Continental Intercalaire et de ses relations avec les autres nappes du Sahara septentrional, Isotop. Tech. Groundw. Hydrol., 1, 227–241, 1975.

Guendouz, A.: Contribution á létude hydrochimique et isotopique des nappes profondes du Sahara nord-est septentrional, Algérie, PhD thesis, Université d'Orsay, Orsay, France, 1985.

Guendouz, A. and Michelot, J.: Chlorine-36 dating of deep groundwater from northern Sahara, J. Hydrol., 328, 572–580, 2006.

Guendouz, A. and Moulla, A.: Étude hydrochimique et isotopique des eaux souterraines de la cuvette de Ouargla, Algérie, Rapport technique, CDTN/DDHI, Algérie, 1996.

Guendouz, A., Moulla, A., Edmunds, W., Zouari, K., Shands, P., and Mamou, A.: Hydrogeochemical and isotopic evolution of water in the complex terminal aquifer in Algerian Sahara, Hydrogeol. J., 11, 483–495, 2003.

Güler, C. and Thyne, G.: Hydrologic and geologic factors controlling surface and groundwater chemistry in Indian wells – Owens valley area, southeastern California, USA, J. Hydrol., 285, 177–198, 2004.

Hadj-Ammar, F., Chkir, N., Zouari, K., Hamelin, B., Deschamps, P., and Aigoun, A.: Hydrogeochemical processes in the Complexe Terminal aquifer of southern Tunisia: An integrated investigation based on geochemical and multivariate statistical methods, J. Afr. Earth Sci., 100, 81–95, 2014.

Hamdi-Aïssa, B., Vallès, V., Aventurier, A., and Ribolzi, O.: Soils and brines geochemistry and mineralogy of hyper arid desert playa, Ouargla basin, Algerian Sahara, Arid Land Res. Manage., 18, 103–126, 2004.

Kenoyer, G. and Bowser, C.: Groundwater chemical evolution in a sandy aquifer in northern Wisconsin, Water Resour. Res., 28, 591–600, 1992.

Kuells, C., Adar, E., and Udluft, P.: Resolving patterns of ground water flow by inverse hydrochemical modeling in a semiarid Kalahari basin, Trac. Model. Hydrogeol., 262, 447–451, 2000.

Le Houérou, H.: Bioclimatology and biogeography of Africa, Springer Verlag, Berlin, Heidelberg, 2009.

Lelièvre, R.: Assainissement de la cuvette de Ouargla, rapports géo-hydraulique no. 2, Ministère des Travaux Publique et de la construction, Algérie, 1969.

Li, P., Qian, H., Wu, J., and Ding, J.: Geochemical modeling of groundwater in southern plain area of Pengyang County, Ningxia, China, Water Sci. Eng., 3, 282–291, 2010.

Ma, J., Pan, F., Chen, L., Edmunds, W., Ding, Z., Zhou, K., He, J., Zhoua, K., and Huang, T.: Isotopic and geochemical evidence of recharge sources and water quality in the Quaternary aquifer beneath Jinchang city, NW China, Appl. Geochem., 25, 996–1007, 2010.

Martinelli, G., Chahoud, A., Dadomo, A., and Fava, A.: Isotopic features of Emilia-Romagna region (North Italy) groundwaters: Environmental and climatological implications, J. Hydrol., 519, 1928–1938, doi:10.1016/j.jhydrol.2014.09.077, 2014.

Matiatos, I., Alexopoulos, A., and Godelitsas, A.: Multivariate statistical analysis of the hydrogeochemical and isotopic composition of the groundwater resources in northeastern Peloponnesus (Greece), Sci. Total Environ., 476–477, 577–590, doi:10.1016/j.scitotenv.2014.01.042, 2014.

Moulias, D.: L'eau dans les oasis sahariennes, organisation hydraulique, régime juridique, PhD thesis, Algérie, 1927.

Moulla, A., Guendouz, A., Cherchali, M.-H., Chaid, Z., and Ouarezki, S.: Updated geochemical and isotopic data from the Continental Intercalaire aquifer in the Great Occidental Erg subbasin (south-western Algeria), Quatern. Int., 257, 64–73, 2012.

OECD: OECD Environmental Outlook to 2030, Tech. Rep. 1, Organisation for Economic Cooperation and Development, Paris, 2008.

ONM: Bulletins mensuels de relevé des paramtres climatologiques en Algérie, Office national météorologique, Ouargla, Algérie, 1975/2013.

OSS: Système aquifère du Sahara septentrional, Tech. rep., Observatoire du Sahara et du Sahel, Tunis, 2003.

OSS: Systme aquifère du Sahara septentrional (Algérie, Tunisie, Libye): gestion concertée d'un bassin transfrontalier, Tech. Rep. 1, Observatoire du Sahara et du Sahel, Tunis, 2008.

Ould Baba Sy, M. and Besbes, M.: Holocene recharge and present recharge of the Saharan aquifers – a study by numerical modeling, in: International symposium – Management of major aquifers, Dijon, France, 2006.

Parkhurst, D. and Appelo, C.: Description of Input and Examples for PHREEQC (Version 3) – A computer program for speciation, batch-reaction, one-dimensional transport, and inverse geochemical calculations, Tech. Rep. 6, US Department of the Interior, US Geological Survey, http://wwwbrr.cr.usgs.gov/ (last access: 15 November 2016), 2013.

Plummer, L. and Back, M.: The mass balance approach: application to interpreting the chemical evolution of hydrological systems., American Journal of Science, 280, 130–142, 1980.

Plummer, L. and Sprinckle, C.: Radiocarbon dating of dissolved inorganic carbon in groundwater from confined parts of the upper Floridan aquifer, Florida, USA, J. Hydrol., 9, 127–150, 2001.

Sharif, M., Davis, R., Steele, K., Kim, B., Kresse, T., and Fazio, J.: Inverse geochemical modeling of groundwater evolution with emphasis on arsenic in the Mississippi River Valley alluvial aquifer, Arkansas (USA), J. Hydrol., 350, 41–55, doi:10.1016/j.jhydrol.2007.11.027, 2008.

Slimani, R.: Contribution à l'évaluation d'indicateurs de pollution environnementaux dans la région de Ouargla: cas des eaux de rejets agricoles et urbaines, MS thesis, Université de Ouargla, Ouargla, 2006.

Stumm, W. and Morgan, J.: Aquatic Chemistry: Chemical Equilibria and Rates in Natural Waters, John Wiley and Sons, New York, 1999.

Thomas, J., Welch, A., and Preissler, A.: Geochemical evolution of ground water in Smith Creek valley – a hydrologically closed basin in central Nevada, USA, Appl. Geochem., 4, 493–510, 1989.

Trolard, F., Bourrié, G., Baillieux, A., Buis, S., Chanzy, A., Clastre, P., Closet, J.-F., Courault, D., Dangeard, M.-L., Di Virgilio, N., Dussouillez, P., Fleury, J., Gasc, J., Géniaux, G., Jouan, R., Keller, C., Lecharpentier, P., Lecroart, J., Napoleone, C., Mohammed, G., Olioso, A., Reynders, S., Rossi, F., Tennant, M., and Lopez, J. D. V.: The PRECOS framework: Measuring the impacts of the global changes on soils, water, agriculture on territories to better anticipate the future, J. Environ. Manage., 181, 590–601, doi:10.1016/j.jenvman.2016.07.002, 2016.

UNESCO: Projet ERESS, Étude des ressources en eau du Sahara septentrional, Tech. Rep. 10, UNESCO, Paris, 1972.

Vallès, V., Rezagui, M., Auque, L., Semadi, A., Roger, L., and Zouggari, H.: Geochemistry of saline soils in two arid zones of the Mediterranean basin. I. Geochemistry of the Chott Melghir-Mehrouane watershed in Algeria, Arid Soil Res. Rehabil., 11, 71–84, 1997.

Zhu, C. and Anderson, G.: Environmental Application of Geochemical Modeling, Cambridge University Press, Cambridge, 139, 596–597, 2002.